Heliyon 9 (2023) e13465

Contents lists available at ScienceDirect

Heliyon

journal homepage: www.cell.com/heliyon

Research article

Effective biosorption of As(V) from polluted water using Fe (III)-modified Pomelo (*Citrus maxima*) peel: A batch, column, and thermodynamic study

Deepak Gyawali [a,b], Sangita Rijal [a], Prabin Basnet [a,c], Kedar Nath Ghimire [a], Megh Raj Pokhrel [a], Hari Paudyal [a,*]

[a] *Central Department of Chemistry, Tribhuvan University, Kirtipur, Kathmandu, Nepal*
[b] *Ministry of Forests and Environment, Department of Environment, Government of Nepal, Nepal*
[c] *Nepal Engineering College, Affiliated to Pokhara University, Changunarayan, Bhaktapur, Nepal*

ARTICLE INFO

Keywords:
Pomelo peel (PP)
Saponification, Fe(III) loading
As(V) biosorption
Interfering ions
Biosorption thermodynamics
Fixed bed column

ABSTRACT

Pomelo, *Citrus maxima*, peel was chemically modified with lime water and then loaded with Fe (III) to develop anion exchange sites for effective sequestration of As(V) from water. Biosorbent characterizations were done by using FTIR, SEM, XRD, EDX, and Boehm's titration. The batch biosorption studies were carried out at various pHs using modified and non-modified biosorbents and optimum biosorption of As(V) occurred at acidic pH (3.0–5.0) for both the biosorbents. A kinetic study showed a fast biosorption rate and obtained results fitted well with the pseudo-second-order (PSO) model. When isotherm data were modeled using the Langmuir and Freundlich isotherm models, the Langmuir isotherm model fit the data better and produced maximal As (V) biosorption capacities of 0.72 ± 03, 0.86 ± 06, and 0.95 ± 05 mmol/g at temperatures 293± 1K, 298± 1K and 303± 1K, respectively. Desorptionof As(V) was effective using 0.1 M NaOH in batch mode. Negative values of ΔG° for all temperatures with positive ΔH° confirmed the spontaneous and endothermic nature of As(V) biosorption. The existence of co-existing chloride (Cl^{-}), nitrate (NO_3^{-}), sodium (Na^{+}), and calcium (Ca^{2+}) showed insignificant interference whereas a high concentration of sulphate (SO_4^{2-}) and phosphate (PO_4^{3-}) significantly lowered As (V) biosorption percentage. Arsenic concentrations in actual arsenic polluted groundwater could be reduced to the WHO drinking water standard (10 μg/L) by using only 1 g/L of investigated Fe (III)-SPP. The dynamic biosorption of As(V) in a fixed bed system showed that Fe(III)-SPP was effective also in continuous mode and different design parameters for fixed bed system were determined using Thomas, Adams-Bohart, BDST, and Yoon-Nelson models. Therefore, from all of these results it is suggested that Fe(III)-SPP investigated in this study can be a potential, low cost and environmentally benign biosorbent material for an effective removal of trace amounts of arsenic from polluted water.

1. Introduction

Arsenic is toxic and classified as a type 1 carcinogenic element, which is a major concern these days due to its negative impact on

* Corresponding author.
E-mail address: hpaudyal@cdctu.edu.np (H. Paudyal).

https://doi.org/10.1016/j.heliyon.2023.e13465
Received 12 October 2022; Received in revised form 25 January 2023; Accepted 1 February 2023
Available online 3 February 2023

human health and destroying the environmental quality. The international Agency for Research on Cancer (IARC) has classified arsenic compounds as Group 1 carcinogens [1]. Arsenic can exist in a variety of oxidation states (−3, 0, +3, and +5) [2], but in natural waters, it is mostly found in the inorganic form as oxyanions of trivalent i.e., As(III) species (H_3AsO_3 at 2–7 pH, $H_2AsO_3^-$ and $HAsO_3^{2-}$ at 7–12 pH, AsO_3^{3-} > 12 pH) called arsenite and pentavalent i.e., As(V) species (H_3AsO_4<2 pH, $H_2AsO_4^-$2-6 pH, $HAsO_4^{2-}$ 6–11.5 pH, and AsO_4^{3-}>11.5 pH) known as arsenate [3–5]. The toxicity of trivalent arsenic is 60 times that of pentavalent arsenic [6]. The As(V) exists in aerobic and oxidizing conditions thus on the earth's surface. It is mostly existed as As(V) in water whereas As(III) is prevalent in anaerobic and moderately reducing conditions [7]. Naturally, the contamination of water with arsenic occurs by the leaching/dissolution of arsenic minerals in a rainy season whereas anthropogenic pollution occurs by various industrial effluents, mining, combustion of fossil fuels, agricultural chemicals, electroplating, pigments, and paints [8–11]. Arsenic polluted surface water is detected in several countries including India, Bangladesh, Chile, China, Mongolia, and Nepal where people are considered to take drinking water containing a high concentration of arsenic [12]. Ingestion of arsenic from polluted water and food is the most common way for humans to be exposed to it [13]. It is accumulated inside our body after the consumption of polluted water through food, vegetables, or drinking [14]. Arsenic poisoning causes a wide range of health problems, including skin leisons and cancers of the liver, kidney, brain, respiratory tract, bladder, and prostate [15,16]. As a result, the United States Environmental Protection Agency (USEPA) and the World Health Organization (WHO) set a maximum contaminant level (MCL) of 10 μg/L of arsenic in drinking water to protect the environment and human health [18]. However, the MCL of arsenic in Nepal is 50 μg/L [17]. Therefore, it is necessary to lower elevated levels of arsenic from polluted water before drinking or discharging into the water bodies.

Nowadays, a variety of techniques are used to remove arsenic from water, including chemical precipitation, reverse osmosis, ion exchange, membrane, nano-filtration, and adsorption [19–23]. The precipitation of arsenic using calcium and iron salts is a commonly used traditional method to reduce arsenic from high concentration however, a large amount of toxic sludge containing huge amount of water is generated in this method which needs further treatment and thus becomes much more problematic and cumbersome [24]. Trace amounts of arsenic, on the other hand, are commonly handled by nanofiltration, ion exchange, and reverse osmosis. Although these methods are effective to lower the arsenic concentration down to the MCL, however, the initial investment and operating cost are too expensive and these techniques are slow [25] thus employment of these methods is inappropriate for the treatment of arsenic-polluted water in developing countries like Nepal. Among multiple treatment processes, adsorption using biomass-based biosorbents looks preferable because of their ease of operation, availability, and economic reasons. Recently most of the research in this field has been devoted to the development of novel, low-cost, high capacity, and environmentally benign adsorbents from the waste biomass of plants and animals. Literature shows that the adsorbent derived from biomass waste such as orange waste, sugarcane bagasse, zee mays, oak wood, activated carbon (AC), cellulose, and chitosan have been reported as effective biosorbents after chemical modification [7,26–29]. Because of the properties such asbiodegradable nature, functional diversity, and ease of chemical modification, the agricultural byproducts-based biosorbent have piqued the interest of many researchers in terms of pollutant uptake in recent years. The Citrus fruits are very polular and the peel of these fruits are rich in pectic substance. Large amount of waste is generated after peeling of these fruits during juicing thus development of new and cost effectivemethod for the utilization of such waste is important.

Pomelo (*Citrus maxima*) is one of the large citrus fruit and is popular in south Asian countries such as Nepal, India, Pakistan, and Bangladesh. In Nepal, the juice of this plant is regarded as delicious and used in making drinks (sharbat) and pickles; which is often eaten as a dessert by dipping in a mixture of chili, salt/sugar, and curd. Pomelo, *C. maxima,* peel (PP) is rich in pectic substances (16–17%) together with cellulose, hemicellulose, lignin, sugar molecules, limonene, minerals, and so on. After harvest, a significant amount of Pomelo peel (PP) waste is produced, which causes growers a number of problems. Therefore, from the viewpoint of economic and environmental concerns, the modification of biopolymer present in PP waste to build natural anion exchanger for arsenic ion removal is a new and effective alternative approach. The success of this endeavor is helpful in that it reduces agricultural waste and provides a natural biosorbent. Therefore, the present research is aimed to develop a natural anion exchange material to sequester As(V) anion by using waste biomass of *C. maxima* peel. Chemically modified *C. maxima* were used to scavenge As(V) from aqueous media in a variety of batch and column tests. Different spectroscopic methods, including scanning electron microscopy (SEM), energy dispersive X-ray (EDX) spectroscopy, Fourier-transform infrared (FTIR) spectroscopy, and X-ray diffraction analysis, as well as chemical analytical methods like Boehm's titration, were used to identify the biosorption mechanism and describe the As(V) biosorption process.

2. Materials and method

2.1. Materials and reagents

Pomelo (*C. maxima*), also called amilo in Nepal, was collected from a farmer in Thankot Kathmandu, a town in the Bagmati province. It was first peeled, repeatedly rinsed with water, chopped into pieces, and let to dry in the sun for a few days. The dried peel of *C. maxima* was then mechanically ground into a fine powder, sieved to allow passage through a mesh size of 150 m, and dried for 24 h in a hot air oven at 363 K. The resulting dried powder was thereafter referred to as Raw Pomelo Peel (RPP).

Three analytical-grade chemicals were used in this experiment: sodium arsenate heptahydrate ($Na_2HAsO_4{\bullet}7H_2O$), calcium hydroxide, and ferric chloride hexahydrate ($FeCl_3{\bullet}6H_2O$). Merck Chemical Co. Ltd. provided the chemicals such as potassium dihydrogen phosphate (KH_2PO_4), sodium chloride (NaCl), sodium hydroxide (NaOH), sodium sulphate (Na_2SO_4), and potassium nitrate (KNO_3). The stock solution of As(V) was prepared by dissolving 2.083 g of $Na_2HAsO_4{\bullet}7H_2O$ with 500 mL of distilled water. The stock solution was diluted at the time of the experiment to make working solutions of As(V) at the necessary concentration. The frequent

dilutions of the stock solutions took place throughout the experiment using double distilled water.

2.2. Preparation of biosorbent from Pomelo Peel (PP)biomass

PP is a non-edible part of Pomelo fruit which have 16–17% of pectin called Pomelo pectin. Each pectin molecule is composed of an ester part and a carboxylic acid part. The methylated ester part of Pomelo pectin was first saponified using lime water to convert them into carboxylic acid groups, then loaded with Fe(III) to develop anion exchange sites for As(V) sequestration. The biosorbent preparation procedure used in this study is similar to that described in Paudyal et al., 2012 with the exception that Fe(III) was loaded onto Pomelo peel biomass rather than loading rare metals in orange waste with minor modifications [30]. First of all, 50 g of dried RPP powder was treated with 500 mL of saturated lime water and stirred for 24 h to saponify the methyl ester part of Pomelo pectin, resulting in saponified Pomelo peel (SPP) as demonstrated in reaction step 1 of Scheme 1.

Since SPP is the calcium salt of Pomelo pectic acid and behaves as a cation exchanger where metal ions can be loaded by cation exchange reaction with Ca(II) ion, however biosorption of anionic species onto this SPP is difficult, thus it needs some further modification to make biosorbent for anionic species. Therefore, SPP was loaded with Fe(III) to develop anion exchange sites for the sequestration of As(V) anions as follows. 10 g of SPP and 250 mL of 0.05 M $FeCl_3 \bullet 6H_2O$ solution (at pH 3) were placed in a 500 mL reaction vessel and shaken for 24 h at 303K. Fe(III) ions that existed in the ferric chloride solution were inferred to be loaded by the substitution of Ca(II) from SPP by cation exchange reaction as shown in reaction step 2 of Scheme 1. It was dried after filtering the mixture and washing the leftover material many times with double-distilled water until getting neutral pH. The dried product obtained in this manner is referred to as Fe(III) loaded SPP and referred to as Fe(III)-SPP, which was employed in the As(V) sequestration during the biosorption experiment.

2.3. Batch biosorption studies

2.3.1. Biosorption test of As(V) using Fe(III)-SPP

The As(V) biosorption and desorption experiments were run in batch mode to examine the effects of pH, kinetics, biosorbent dosage, and isotherms. Twenty five mililiter of solution containing 0.062 mmol/L of As(V) was mixed with 40 mg of biosorbents (RPP, SPP, and Fe(III)-SPP) at various pHs ranging from 1 to 12 to assess the effect of pH on As(V) biosorption. The solutions were filtered after 24 h and the final pH values were recorded. Kinetic studies were conducted to determine the shortest time required for the system to reach equilibrium. At optimal pH, 40 mg of biosorbent and 25 mL As(V) solution (0.063 mmol/L) were agitated for various intervals of time ranging from 5 to 300 minutes. The biosorption isotherm tests were carried out by shaking biosorbent and As(V) solution at varying concentrations at solid liquid ratio of 1.6 g/L keeping other parameters constant. Despite the fact that the biosorption's equilibrium period was discovered to be 6 h, the solid-liquid mixture was agitated for 24 h in the studies that followed to assure full

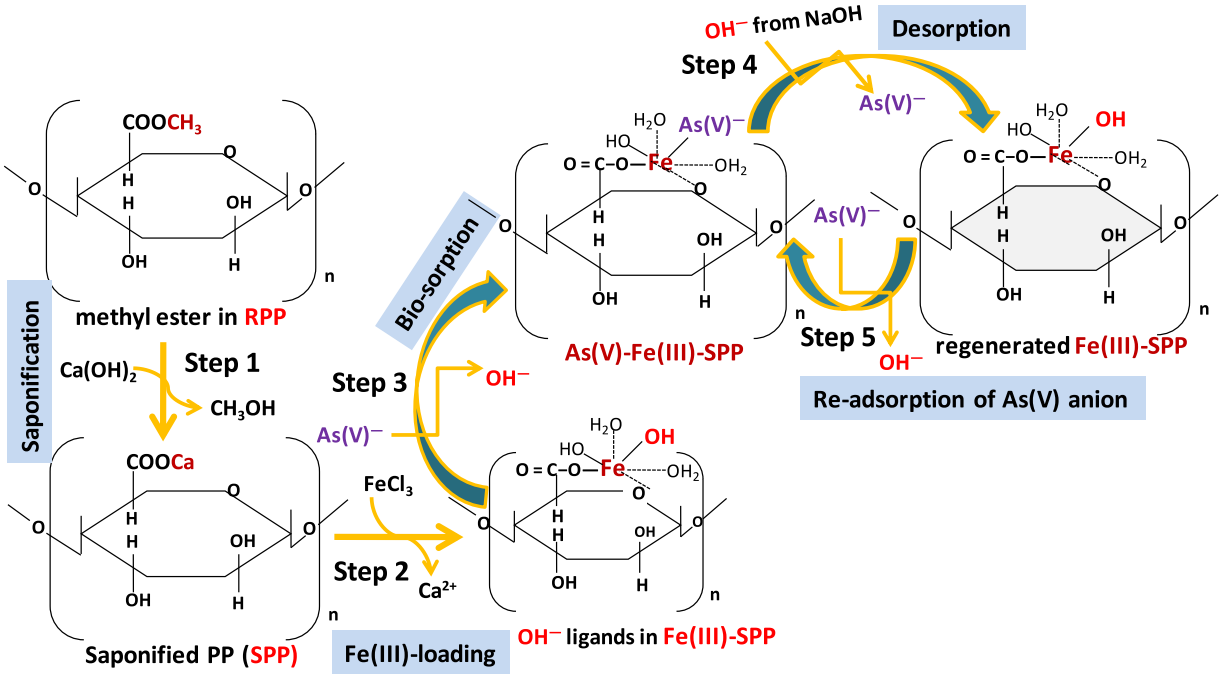

Scheme 1. Synthetic route of Fe(III)-SPP biosorbent from RPP by $Ca(OH)_2$ treatment followed by Fe(III) loading and its As(V) biosorption, desorption and re-generation mechanism.

equilibrium. The effect of biosorbent dosage was investigated by changing the amount of Fe(III)-SPP (0.5–4 g/L) by using 3 different arsenic-contaminated groundwater samples collected from the Nawalparasi district. After shaking at predetermined interval of time, it was filtered and the concentration of As(V) solution before and after biosorption was measured. The % of biosorption and amount of As (V) uptake were calculated according to the following mass-balance relationships

$$\%A = \frac{C_i - C_e}{C_i} \times 100 \tag{1}$$

$$q = \frac{C_i - C_e}{W} \times V \tag{2}$$

Where, q is the uptake amount of As(V) (mmol/g), C_i and C_e are the As(V) concentration before and after biosorption (mmol/L), respectively, W is dry weight of biosorbent (g) and V is the volume of adsorbate solution in a liter.

2.3.2. Desorption test of As(V) anion

Prior to the desorption test, the As(V)-loaded Fe(III)-SPP was prepare by agitating 1 g of Fe(III)-SPP with 500 mL of As(V) solution (1.33 mmol/L) at the optimal pH for 24 h. The residue was then filtered and washed many times with distilled water before being dried. The product obtained in this way is called As(V)-loaded Fe(III)-SPP and abbreviated as As(V)–Fe(III)-SPP hereafter. To determine which desorbing solution would be best, a preliminary desorption test was conducted using neutral (1 M NaCl), basic (1 M NaOH), and acidic (1 M HCl) solutions. It was found that HCl destroyed the active sites by leaching loaded Fe(III) from Fe(III)-SPP, NaCl is not effective (it desorbed <25% of As(V)) and NaOH was found to be effective (it desorbed >98% of As(V)) during desorption process. Thus further optimization was done using NaOH solution as follows. For this, 10 mL of NaOH solution at various concentrations (0.05–2 M) were shaken for 6 h with 50 mg of As(V)–Fe(III)-SPP. Then it was filtered and the filtrate was analyzed for arsenic ion to determine the desorbed amount of As(V). The percentage of As(V) desorbed from the As(V)–Fe(III)-SPP was calculated using the following relationships as [31].

$$\%\ \text{Desorption} = \frac{D_{amount}}{A_{amount}} \times 100 \tag{3}$$

Where A_{amount} (mmol/g) and D_{amount} (mmol/g) are the amount of As(V) sorbed onto Fe(III)-SPP and desorbed amount, respectively.

2.3.3. Determination of acidic functional groups

Boehm's titration procedure, described elsewhere [22], was used to estimate the amount of carboxyl, phenolic, and lactonic groups on the biosorbent surface. In four separate stopper bottles, 0.5 g of Fe(III)-SPP was mixed with 25 mL (0.05 M, each) of NaOH, $NaHCO_3$, Na_2CO_3, and HCl. After a 24 h shaking, the mixture was then filtered and analyzed to determine the adsorbed amount of As(V). NaOH, is the strong base and is thought to neutralize all Brønsted acids, whereas Na_2CO_3 and $NaHCO_3$ are said to be neutralizing carboxylic and lactonic groups, respectively [22]. After that, the filtrates were back-titrated against 0.05 M NaOH with an excess (10 mL) of 0.05 M HCl.The amount of $NaHCO_3$ consumed by the sample was used to calculate the carboxylic acid group concentrations on the Fe (III)-SPP surface. The amount of the lactonic group was determined by subtracting the amounts of Na_2CO_3 and $NaHCO_3$ consumed by the sample whereas that of the phenolic group was determined by subtracting the amounts of NaOH and Na_2CO_3 consumed by the sample.

2.4. Dynamic biosorption of As(V) in fixed bed column of Fe(III)-SPP

Compared to a batch study, the biosorption test in a fixed bed system offers a number of advantages for use in practical situations. A solution with a fixed initial concentration is passed over the biosorbent bed in a dynamic system. The fixed bed column experiments were carried out in a glass column that was 20 cm in height with an interior diameter of 8 mm. Using a peristaltic pump, As(V) solution (0.061 mmol/L) was percolated from the bottom of column at a constant flow rate of 150 mL/h. An automatic sample collector was used to collect the effluent samples every hours. The experiment was carried out until the As(V) concentrations in effluent solution is identical with influent solution. The following equations were used to calculate the different column parameters [32].

The total amount of As(V) biosorbed onto the column

$$(q_{total}) = \frac{\mathrm{F\,A}}{1000} = \frac{\mathrm{F}}{1000} \times \int_{t_0}^{t_T} C_{ads}\,dt \tag{4}$$

$$\text{Effluent volume } (\mathrm{Eff_{volume}}) = \mathrm{F\ t_T} \tag{5}$$

$$\text{Equilibrium As(V) sorption capacity } (\mathrm{q_{column}}) = \mathrm{q_{total}\ /\ M} \tag{6}$$

$$\text{Mass transfer zone } (\Delta t) = \mathrm{t_e - t_b} \tag{7}$$

Where, F (mL/h) is flow rate, A (cm^2) is area of breakthrough curve, and M (g) is the mass of the biosorbent whereas t_e, t_b, and t_T are exhaustion, breakthrough, and total flow times in hours, respectively.

2.5. Statistical analysis

The reproducibility of the data in repeated biosorption test is very important to validate the investigated results in the scientific community. To determine mean, standard deviation, and other statistical indicators such as Chi-square test (χ^2), root-mean-square error (RMSE), and mean absolute error, three sets of experimental results from a triplicate studies of As(V) sequestration were statistically examined. The following equations (Eq. (8) to Eq. (10)) represent the mathematical formulation for their determination [31].

$$\chi^2 = \sum \frac{(q_{m.e} - q_{m.c})2}{q_{m.c}} \tag{8}$$

$$\mathrm{RMSE} = \sqrt{\left[\frac{\sum_{i=1}^{n}(q_{m.e} - q_{m.c})2}{n}\right]} \tag{9}$$

$$\mathrm{MAE} = \left(\frac{1}{n}\right)\sum_{i=1}^{n}|q_{m.e} - q_{m.c}| \tag{10}$$

Where, $q_{m.\ e}$ is experimental value of maximum As(V) uptake capacity and $q_{m.\ c}$ is As(V) uptake capacity calculated from best fit isotherm or kinetic models in mmol/g, respectively. Lower value of these error function provides the evidence that calculated values from examined mathematical models closely resembled to the experimental data.

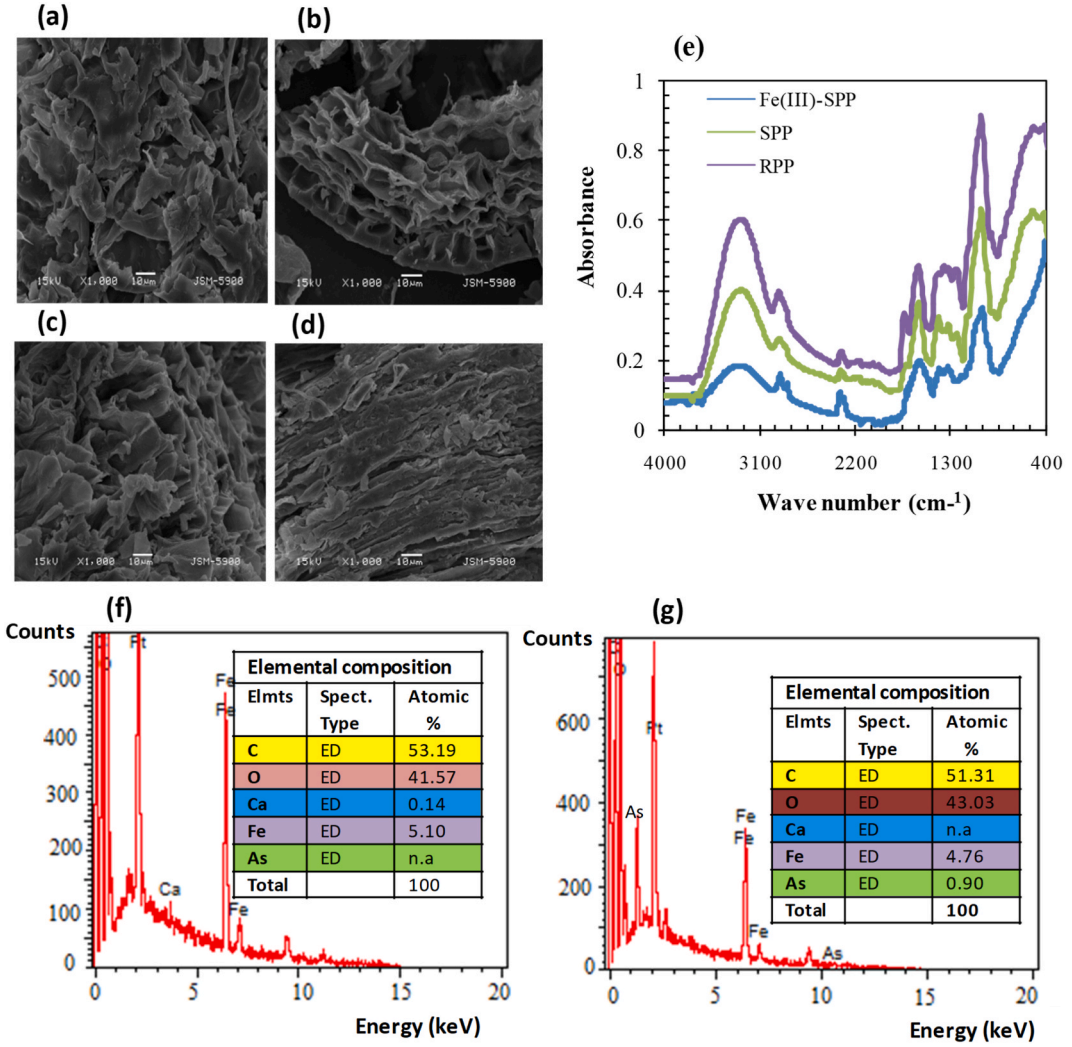

Fig. 1. Surface morphology, FTIR charecterizations and EDX spectra of pomelo based biosorbents (a–d) SEM images of RPP, SPP, Fe(III)-SPP and Fe (III)-SPP after As(V) biosorption, (e) FTIR spectra of RPP, SPP and Fe(III)-SPP and (f and g) EDX spectra of Fe(III)-SPP before and after As(V) biosorption.

2.6. Analytical setup and instrumentation

The functional group modification of feed material during saponification and Fe(III) loading were analyzed by using FTIR spectrophotometer (IR Affinity-1S-SHIMADZU spectrometer, Kyoto, Japan). The spectral datas were recorded at wave number range from 4000 to 400 cm^{-1} with resolution of 4 cm^{-1}. The change in surface microstructure of biosorbent was determined by using a SEM (JEOL JSM 5900) whereas that of elemental compositions was investigated using an EDX spectrometer. To determine As(V) concentration before and after biosorption, AAS (Perkin Elmer, USA) and an ICP-MS (ICP-MS, Agilent 7900, Santa Clara, CA, USA) were used. The crystalline property of the biosorbent was determined by using X-ray diffractometer in the 2Θ range of 10–80° by using Cu–Kα (λ = 1.54056 Å) radiation (Rigaku Company, Japan).

The pH meter (CHEMI LINE CL-180) was used to determine the solution's pH. An Iwaki model 100 N peristaltic pump was used to regulate the feed solution's flow rate, and a sample collectior (Bio-Rad model-2110) was used to collect effluent samples.

3. Results and discussion

3.1. Instrumental characterizations

The surface morphology change observed in RPP before and after saponification is clearly shown in Fig. 1(a) and (b). The majority of the RPP surface is smooth but contains some shining patches heterogeneously (Fig. 1(a)) whereas the surface becames much rough and had many ups and downs after saponification in case of SPP (Fig. 1(b)) which may be due to the loss of some low molecular limonene and sugar molecules from the RPP surface. Fig. 1(c) and (d) shows the SEM images of Fe(III)-SPP before and after As(V) biosorption. Fe(III)-SPP surface is quite smooth than SPP (Fig. 1(c)); however, it became much more smooth and all the ups and downs surfaces were covered by a shining layer showing the drastic change in surface morphology after As(V) biosorption (Fig. 1(d)) which might be caused by the coating of biosorbed As(V) on the surface of Fe(III)-SPP. A similar change in surface morphology is also observed in case of TiO_2 modified pomegranate peel (TiO_2@PP) and La(III) modified watermelon rind (La(III)-SWR) in previous researchs after As(V) biosorption [31,34].

FTIR is a useful spectroscopic tool to analyze the functional groups responsible for the chemical modification during biosorbent synthesis and As(V) biosorption. Fig. 1(e) depicts the FTIR spectra of RPP, SPP, Fe(III)-SPP, and As–Fe(III)-SPP in absorption mode. In RPP, peak observed at 3420, 2921, 1730, 1573, and 1170 cm^{-1} are due to stretching vibration of O–H, C–H, C═O, C═C, and C–O bonds, respectively [35,36]. The peak observed at 1018 cm^{-1} is due to C–*O*–C stretching of ester and other lignocellulosic groups. The observation of the various peaks in the FTIR spectra demonstrates the existence of varieties of functional groups in the RPP surface. Peak intensity of OH, C–H, and C═O are found to be higher than others sothat these are the major functional groups in the feed material.

In case of SPP, the peak at 3420 cm^{-1} became wide and shifted to 3409 cm^{-1}. The peak position of C–H at 2920 cm^{-1} remained unchanged even after saponification from which it can be concluded that alkane groups played no significant role in saponification reaction. Peaks appeared at 1720 cm^{-1} due to C═O stretching vanished after $Ca(OH)_2$ treatment and new peaks related to metal carboxylates, in this case, calcium carboxylate, appeared at wave number around 1667 cm^{-1} and 1481 cm^{-1}, which clearly explains the major role of carboxylic acid functional groups of RPP during saponification reaction. The peaks related to calcium carboxylate at 1667 cm^{-1} became much broader and extended from 1836 to 1492 cm^{-1} in Fe(III) loaded SPP which might be due to the binding of high molecular ferric ions by replacing lighter calcium ion *via* cation exchange mechanism as depicted by Scheme 1 (step 2). All of these results suggested that the major chemical modification occurred in the carboxylic acid functional group of Pomelo peel biomass during biosorbent synthesis.

The crystalline nature of biosorbents is considered to be changed during chemical modification. For this, the XRD spectra of RPP (feed material) and Fe(III)-SPP are compared as shown in Supplementary Fig. 1 (Fig. S1). Crystalline structure of cellulose is indicated from the clear and intense peaks observed at 2θ values around 12.10, 13.40, 19.23, 25.13, and 38.65 in RPP sample which are disappeared in Fe(III)-SPP and two broad peaks extending at 2θ values from 13.24 to 18.59 and 19.24 to 25.17 are appeared. The results suggest an improvement in the amorphous nature of biosorbent after chemical modification which is expected to be more suitable for As(V) biosorption.

Fig. 1(f) and (g) show the observed EDX spectra of Fe(III)-SPP before and after As(V) biosorption. It shows that the strong peaks due to C and O elements are observed at binding energies of 0.27 and 0.53 keV, respectively together with Ca (3.69 keV and 4.12 keV) and Fe (6.39 keV and 7.14 keV) in Fe(III)-SPP (Fig. 1(f)), whereas new peaks due to arsenic element (**As**) is appeared at the binding energies of 1.28 keV and 10.53 keV in As(V) treated Fe(III)-SPP (Fig. 1(g)) in addition to the all the peaks of Fe(III)-SPP. The analysis of elemental composition showed that there is a lack of **As** element in the sample of Fe(III)-SPP whereas 0.90% of **As** existed in As(V)–Fe(III)-SPP. This finding implies that the As(V) is effectively biosorbed by Fe(III)-SPP. Moreover, the amount of oxygen content in Fe(III)-SPP is found to be increased from 41.57% to 43.03% together with the appearance of new peak of **As** (0.90%) after biosorption. Such a appearance of a new elemental peak of **As** and an increase in the amount of oxygen implying that the complex ion containing **As** and **O** is biosorbed onto Fe(III)-SPP during As(V) biosorption. A similar types of biosorption behavior was investigated by Poudel et al., 2020 in the case of As(III) adsorption using TiO_2@PP [36].

3.2. Amount of acidic functional groups

Using Boehm's titration, it is discovered that SPP contains 2.5, 1.75, and 2.74 mol of carboxylic, lactonic, and phenolic functional

groups per kilogram of biosorbent, respectively.

3.3. Batch-wise biosorption and desorption

3.3.1. Influence of pH and mechanism of As(V) biosorption

The pH is one of the controling biosorption parameters that potentially affect the As(V) uptake process because the surface charge of the biosorbent and arsenic speciation changes with pH variation [37,38]. The surface of the biosorbent is negatively charged at pH levels above pHpzc and positively charged at pH levels below pHpzc. Literature showed that As(V) exists as H_3AsO_4 (<2 pH), $H_2AsO_4^-$ (2–6 pH), $HAsO_4^{2-}$ (6–11.5 pH) and AsO_4^{3-} (>11.5 pH) species [38] (supplementaryfigure2a,Fig. S2a). The relation between the % biosorptions of RPP, and Fe(III)-SPP for As(V) as a function of equilibrium pHs are shown in Fig. 2. It shows that biosorption of As(V) onto RPP, feed material, is less than 5% and that of SPP is not higher than 10% even at optimum pH however it is drastically improved after Fe(III) loading (92.4% at pH 2.14). The biosorption of As(V) by RPP (feed material, only 4.9% at 7.03 pH) and SPP (6.8% at equilibrium pH 10.43) (Supplementary Fig. 2b, Fig. S2b) is too poor or insignificant.

In the case of Fe(III)-SPP, the As(V) biosorption increased from 61.3% to 80.32% with the increase of equilibrium pH from 0.73 to 1.08 and reached a maximum value (92.4%) at 2.14 pH, then decreased with further increase of equilibrium pH, which is reasonably ascribed due to the creation of new ligand exchange sites for As(V) anion after Fe(III) loading reaction. Influence of pH for the sequestration of As(V) onto Fe(III)-SPP can be better understood from the As(V) distribution in solid phase by evaluating distribution coefficient (K_D) using following equation [31].

$$K_D = \frac{C_i - C_e}{C_e} \times \frac{V}{W} \tag{11}$$

Where K_D is distribution coefficient and W is the weight of the Fe(III)-SPP used. Supplementary Fig. 2c, Fig. S2c shows the K_D value of biosorbed As(V) onto the surface of RPP and Fe(III)-SPP at different pH. It shows that the distribution of As(V) is maximum at optimum pH for both the biosorbents, which further confirmed that As(V) biosorption by Pomelo-based biosorbents is highly pH dependent. Investigated results are in agreement with some other publications for the biosorption of arsenic using different kinds of biosorbents [36–38]. Furthermore, a drastic increase of K_D value of As(V)–Fe(III)-SPP compared to RPP strongly suggested the improvement in biosorption performance of As(V) after modification, which is because of the development of new active sites for As(V) removal *via*. Fe (III) loading. The creation of active sites can be explained as follows. Due to steric hindrance caused by the massive Pomelo Pectic Acid (PPA) molecule, neutralizing all three positive charges of Fe(III) with the carboxyl group of PPA is not possible. As a result, one or two positive charges of the ferric ion are neutralized by the carboxyl group(s) of PPA, and the remaining positive charges are neutralized by the hydroxyl ion in aqueous solution, which was inferred to be substituted by As(V) anion during the biosorption process (step 3, Scheme 1). Isoelectric point or pH_{PZC} value for Fe(III)-SPP biosorbent from pH drift experiment is determined to be around 7(Supplementary Fig. 2d, Fig. S2d) thus biosorption of As(V) anion has favoured below this pH because the surface positive charge of Fe (III)-SPP provides a driven force for the interaction of As(V) anion by coulombic force of attraction.

At higher pH, the hydroxyl groups that existed on the surface of the biosorbent are deprotonated yielding a negative surface, thus As (V) biosorption displayed an obvious decreasing trend due to coulombic repulsion between As(V) anions and negatively charged Fe (III)-SPP surface. In addition to this, the decreasing trend of % biosorption of As(V) at higher pH is resonably attributed because of the increasing concentration of competing OH ions for the same ligand exchange sites.

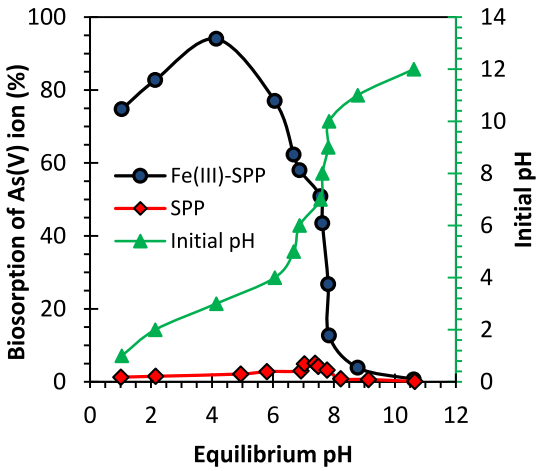

Fig. 2. Influence of solution pH for the biosorption of As(V) onto SPP and Fe(III)-SPP
(Conditions: weight of biosorbent = 40 mg, volume of solution = 25 mL, As(V) concentration = 0.062 mmol/L, shaking time = 24 h, and shaking speed = 200 rpm).

3.3.2. Biosorption kinetics

The influence of contact time on As(V) biosorption onto Fe(III)-SPP is shown in Fig. 3. As can be seen that the biosorption of As(V) is rapid at the beginning then it slowed down and reached equilibrium within 120 min. The sharp biosorption curve suggests that the biosorption occurred rapidly in the initial stage on the surface of Fe(III)-SPP, it is because of the existence of a large number of vacant sites. Uptake of As(V) gradually decrease and finally attains equilibrium.

After examining experimental data using the Weber and Morish intraparticle diffusion (IPD), pseudo-first-order (PFO), and pseudo-second-order (PSO) models, the best fitted kinetic model for the biosorption of As(V) is determined. The nonlinear and linear equations for the PFO model are, respectively, expressed in Equation (12) and Equation (13) as [39,40].

$$q_t = q_e\left(1 - e^{-k_1 t}\right) \rightarrow \text{non} - \text{linear} \tag{12}$$

$$\log(q_e - q_t) = \log q_e - \frac{k_1}{2.303} t \rightarrow \text{linear} \tag{13}$$

Where q_e and q_t are the biosorption capacity at equilibrium (mmol/g) and at time t (min), respectively, and k_1 is the PFO rate constant (min^{-1}). The linear plot of $\log(q_e - q_t)$ versus t (time) is created (Supplementary Fig. 3a, Fig. S3a), from which the values of k_1 (0.61×10^{-3} min^{-1}) and q_{e1}, 0.062 ± 0.009 mmol/g) are calculated using slope and intercept, respectively, and the evaluated values are presented in Table 2. Equations (14) and (15) can be used to express the pseudo-second-order (PSO) model [41,42].

$$q_t = \frac{k_2 q_e^{\,2} t}{1 + k_2 q_e t} \rightarrow \text{non} - \text{linear} \tag{14}$$

$$\frac{t}{q_t} = \frac{1}{k_2 q_e^{\,2}} + \frac{1}{q_e} t \rightarrow \text{linear} \tag{15}$$

For the PSO model, k_2 and q_{e2} are the rate constant and computed biosorption capacity, respectively. Slope and intercept obtained from the plots of t/q_t *vs* t (Supplementary Fig. 3b, Fig. S3b) are used to calculate uptake capacity for PSO model and intercept is used to evaluate PSO rate constant k_2. Similarly, the Weber and Morish model for intraparticle diffusion (IPD) can be written as [43].

$$q_t = k_{IPD} \times \sqrt{t} + C \tag{16}$$

k_{IPD} is the IPD rate constant, and C is constant. The plot of q_t versus t (Supplementary Fig. 3c, Fig. S3c), depicts the three distinct regions in the plot, the first being a sharp increase in q_t, the second being a gradual or slight increase, and the third being a plateau value. The result shows that q_t increases over time in three different ways.

Table 1 shows the results of kinetic parameters evaluated using the PFO, PSO, and IPD models. It is obvious from this table that the PSO model ($R^2 = 0.99$) fits the observed As(V) biosorption data better than the PFO ($R^2 = 0.94$) and IPD ($R^2 = 0.97$) which have lower values of coefficient of determination. The As(V) uptake capability of Fe(III)-SPP was determined for additional validation using the nonlinear equation of PFO, PSO and IPD and the evaluated values are plotted togetter with experimental results for comparison as shown in Fig. 3. The outcome of this result demonstrates that the biosorption amount estimated using the PSO model ($q_{e2} = 0.091 \pm$

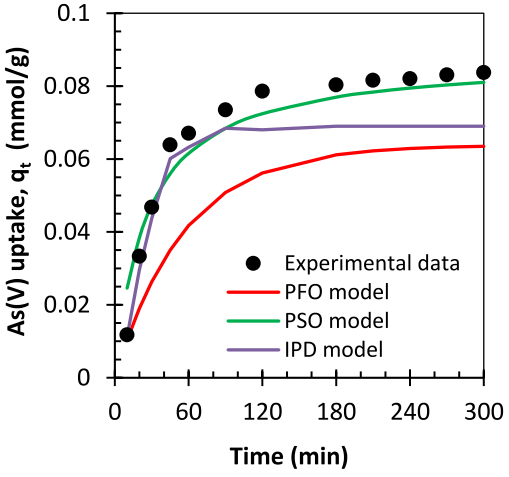

Fig. 3. Experimental results showing the biosorption kinetics of As(V) onto Fe(III)-SPP together with the non-linear modeling using PFO, PSO and IPD model.
(Conditions: weight of biosorbent = 40 mg, volume of solution = 25 mL, As(V) concentration = 0.063 mmol/L, shaking time = 24 h, and shaking speed = 200 rpm).

Table 1
Kinetics parameters for the adsorption of As(V) onto Fe(III)-SPP

Kinetic models	Kinetic parameters	Evaluated values
As(V) uptake capacity (experimental)	q_{exp}. (mmol/g)	0.084 ± 0.004
Pseudo first order (PFO) model	$k_1 \times 10^{-3}$ (1/min)	0.61 ± 0.022
	q_e, cal. (mmol/g)	0.062 ± 0.009
	R^2	0.94
	$\chi^2 \times 10^{-2}$	0.78 ± 0.04
	RMSE $\times 10^{-3}$	0.48 ± 0.003
	MAE $\times 10^{-2}$	2.2 ± 0.23
Pseudo second order (PSO) model	k_2 (g/(mmol min))	0.24 ± 0.002
	q_e, cal. (mmol/g)	0.091 ± 0.004
	R^2	0.99
	$\chi^2 \times 10^{-2}$	0.053 ± 0.008
	RMSE $\times 10^{-3}$	0.049 ± 0.006
	MAE $\times 10^{-2}$	0.7 ± 0.005
Intra particle diffusion (IPD) model	q_e, cal. (mmol/g)	0.069 ± 0.007
	k_{IPD1} (mmol/g)	0.014 ± 0.004
	R^2	0.97
	$\chi^2 \times 10^{-2}$	0.32 ± 0.047
	RMSE $\times 10^{-3}$	0.22 ± 0.014
	MAE $\times 10^{-2}$	1.5 ± 0.057

Table 2
Evaluated isotherms parameters for the sorption of As(V) onto investigated Fe(III)-SPP adsorbent at pH 4.

Isotherm parameters		SPP	Fe(III)-SPP		
		298K	293K	298 K	303 K
Langmuir	q_{exp}(mmol/g)	0.12 ± 0.07	0.69 ± 0.07	0.84 ± 0.10	0.93 ± 0.09
	q_{max}(mmol/g)	0.11 ± 0.06	0.72 ± 0.06	0.86 ± 0.08	0.95 ± 0.05
	b (L/mmol)	2.67 ± 0.12	2.78 ± 0.16	4.47 ± 0.35	6.68 ± 0.16
	R^2	0.98	0.99	0.99	0.99
	$\chi^2 \times 10^{-2}$	0.90 ± 0.002	0.041 ± 0.002	0.023 ± 0.005	0.021 ± 0.003
	RMSE $\times 10^{-3}$	0.1 ± 0.58	9 ± 0.58	4 ± 0.37	4 ± 0.26
	MAE	0.01 ± 0.001	0.03 ± 0.001	0.02 ± 0.003	0.02 ± 0.002
Freundlich	K_F (mmol/g) (L/mmol)$^{1/n}$	0.06 ± 0.003	0.41 ± 0.07	0.56 ± 0.12	0.66 ± 0.17
	n	3.06 ± 0.56	2.81 ± 0.56	3.38 ± 0.84	3.70 ± 0.39
	R^2	0.94	0.92	0.91	0.95
	$\chi^2 \times 10^{-2}$	7.51 ± 0.24	7.51 ± 0.24	4.61 ± 0.13	3.65 ± 0.29
	RMSE	0.36 ± 0.018	0.36 ± 0.018	0.47 ± 0.013	0.53 ± 0.011
	MAE	0.61 ± 0.025	0.61 ± 0.025	0.69 ± 0.014	0.73 ± 0.017
Temkin	q_e (mmol/g)	0.068 ± 0.07	0.38 ± 0.04	0.42 ± 0.08	0.44 ± 0.05
	b_T (J g/(mol)^2)	123878.60 ± 122.39	21750.02 ± 97.23	21544.10 ± 41.71	21716.74 ± 44.97
	B (mmol/g)	0.02 ± 0.0013	0.112 ± 0.0018	0.115 ± 0.0015	0.116 ± 0.0021
	A_T	49.40 ± 3.79	77.34 ± 7.41	231.24 ± 12.16	564.65 ± 19.35
	R^2	0.95	0.96	0.97	0.97
	χ^2	7.51 ± 0.24	7.51 ± 0.24	4.61 ± 0.13	3.65 ± 0.29
	RMSE	0.36 ± 0.018	0.36 ± 0.018	0.47 ± 0.013	0.53 ± 0.011
	MAE	0.61 ± 0.025	0.61 ± 0.025	0.69 ± 0.014	0.73 ± 0.017

0.004 mmol/g) is much closer to the experimental value ($q_{exp} = 0.084 \pm 0.006$ mmol/g) than the PFO ($q_{e1} = 0.062 \pm 0.009$ mmol/g) and IPD ($q_{eIPD} = 0.069 \pm 0.007$ mmol/g) models. Therefore from all the results, it is suggested that the rate-limiting phase could be chemisorptions that involves the sharing or transfer of electrons between the ligand exchange sites of Fe(III)-SPP and As(V) anion during the biosorption process. Past studies also reported that the As(V) biosorption preferentially follows PSO model rather than PFO and Weber and Morish IPD models [35,36].

3.3.3. *Equilibrium biosorption isotherm*

The mathematical models that describe how the sorbate species are distributed in a solid and liquid phase at equilibrium is known as biosorption isotherm. Fig. 4(a)–(d) shows the plots of the equilibrium biosorption capacity of AS(V) as a function of residual concentration together with the nonlinear modeling of Langmuir, Freundlich, and Temkin isotherms. The result revealed that As(V) uptake capacity of SPP at 298K (Figs. 4(a), 0.12 ± 0.07 mmol/g) is drastically improved after Fe(III) loading (Figs. 4(c), 0.84 ± 0.10 mmol/g) which might be due to the creation of the new ligand exchange sites for As(V) *via* Fe(III) loading. The uptake of As(V) increased with increasing temperature (Fig. 4(b)–4(d)), indicating the endothermic nature of biosorption, which will be further prooved by analyzing thermodynamic parameters. At lower concentrations, the As(V) biosorption capacity of SPP and Fe(III)-SPP increased with increasing As(V) concentration, but at higher concentrations, it became constant or flat. This plateau value is used

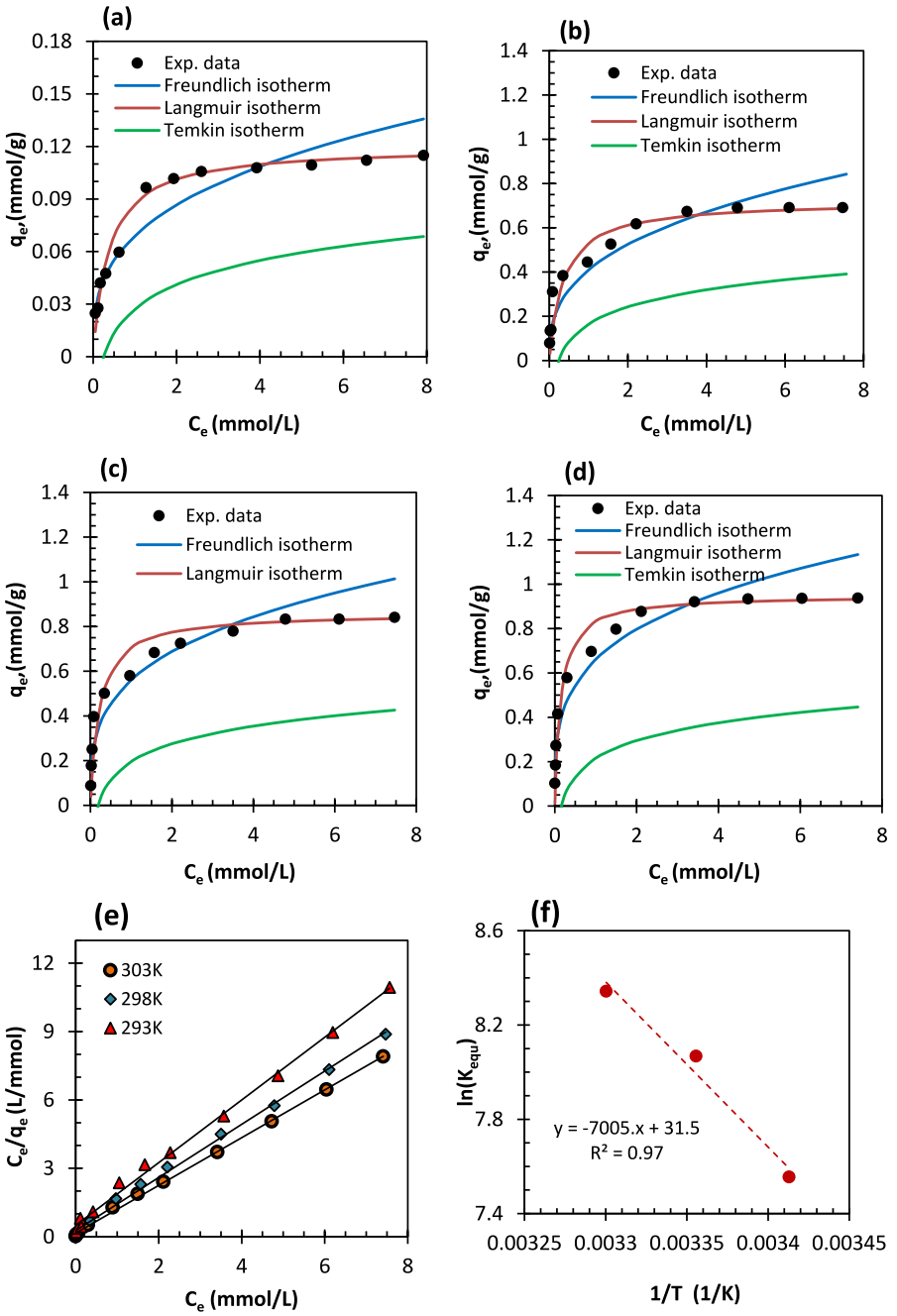

Fig. 4. Biosorption isotherm of As(V) using (a) SPP at 298K and (b, c, and d) Fe(III)-SPP at different temperatures (e) linear plots obtained from Langmuir isotherm model and (f) Vant Hoff's plot.
(Conditions: weight of biosorbent = 40 mg, volume of solution = 25 mL, pH = 4 ± 0.1, shaking time = 24 h, and shaking speed = 200 rpm).

to calculate the experimental biosorption capacity (q_{exp}). To investigate the best-fit isotherm model, Freundlich, Langmuir, and Temkin isotherm models are utilized. Langmuir model is the most often used isotherm to describe the biosorption data and evaluatethe biosorption equilibrium constant and maximum biosorption capacity. Equations (17) and (18) below can be used to express the nonlinear and linear forms of Langmuir isotherms, respectively [44,45].

$$q_e = \frac{q_{max} b C_e}{1 + bC_e} \tag{17}$$

$$\frac{C_e}{q_e} = \frac{1}{q_{max}\, b} + \frac{1}{q_{max}} C_e \tag{18}$$

where q_e is the amount of As(V) biosorbed (mmol/g) at equilibrium, C_e is the equilibrium concentration (mmol/L), q_{max} is the maximum amount of As(V) sorbed onto the investigated biosorbents, and b (L/mmol) is the biosorption equilibrium constant related to binding energy. Slope and intercept obtained from the plot of C_e/q_e *vs* C_e (Fig. 4(e)) are used to estimate the maximum biosorption capacities (q_{max}, of 0.72 ± 06, 0.86 ± 08, and 0.95 ± 05 mmol/g) and biosorption equilibrium constant (b, 2.78 ± 0.12, 4.47 ± 0.35, 6.68 ± 0.16, L/mmol) at temperatures 293, 298 and 303K, respectively. In a similar way, the Freundlich isotherm equation can be written in both linear (Eq. (20)) and nonlinear (Eq. (19)) versions as [46–48].

$$q_e = K_F C_e^{1/n} \tag{19}$$

$$\log q_e = \log K_F + (1/n) \log C_e \tag{20}$$

Freundlich constants K_F and n are related to biosorption potential and biosorption intensity, respectively. K_F and n are estimated from the intercept and slope of the log (q_e) *vs* log (C_e) plots (Supplementary Fig. 4a, Fig. S4a), respectively for all temperatures. Both the nonlinear (Eq. (21)) and linear (Eq. (22)) formulations of the Temkin isotherm can be express as [49].

$$q_e = B \ln(AC_e) \text{ and } B = \frac{RT}{b_T} \tag{21}$$

$$q_e = \frac{RT}{b_T} \ln A + \frac{RT}{b_T} \ln C_e \tag{22}$$

where R (8.314 J/mol K), T (K), and b_T (kJ/mol) are universal gas constant, absolute temperature and Temkin constant, respectively. Temkin plot (Supplementary Fig. 4b, Fig. S4b) of q_e versus ln(C_e) is used to estimate the value of b_T, and A using slope and intercept, respectively. Table 2 provides the values for isotherm parameters determined using the Langmuir, Freundlich, and Temkin isotherm models. It is evident from the results of this table that the Langmuir isotherm model yielded a greater cofficient of determination ($R^2 >$ 0.99) compared to Freundlich ($R^2 = <0.95$) and the Temkin model ($R^2 < 0.97$), thus biosorption of As(V) is inferred to occur according to the Langmuir monolayer adsorption theory. To make a further confirmation, the As(V) biosorption capacity calculated using the nonlinear modelling of Langmuir, Freundlich, and Temkin models are plotted alongwith experimental uptake capacity as shown in Fig. 4(a)–(d). Equilibrium biosorption capacity (q_e) computed using the Freundlich and Temkin isotherm model did not agree with the experimental q_e value, however, the q_e value determined using the Langmuir isotherm did for all the cases. Thus the obtained results are in good agreement to the experimental finding. All of these finding potentially suggest the formation of monolayer of As(V) on the surface of Fe(III)-SPP during As(V) sequestration process.

Table 3 shows the comparison of maximum biosorption potentials of different biosorbents reported for As(V) with the investigated Fe(III)-SPP [33,37,50–61]. The result shows that the As(V) uptake capacity of nonmodified jute fiber, CuO-treated biochar, iron-impregnated *Citrus limenta*, iron-treated sawdust, etc has low biosorption potential whereas biosorbent loaded with a transition metal, and metaloxide/or hydroxide such as magnetic orange peel, Fe_2O_3 treated jute fiber, ferric oxide modified sugarcane bagasse, Fe-Zr binary oxide, and Zr(IV) loaded orange waste have high biosorption potential. Arsenic has a high affinity towards iron thus Fe (III) loaded biosorbents shows high selectivity towards arsenic ion. Fe(III)-SPP investigated in this research work has satisfactory biosorption potential among the reported biosorbents in Table 3. As a result, the Fe(III)-SPP studied in this research work can be used as a low-cost, efficient, arsenic-selective, and environmentally safe material, and might be better option for the treatment of

Table 3
Maximum As(V) uptake capacity of Fe(III)-SPP and SPP with other reported adsorbents.

Adsorbent	pH	$q_{max.}$ (mmol/g)	Reference
Fe(III)-SPP at 293K	4.0	0.73	This work
Fe(III)-SPP at 298K	4.0	0.86	This work
Fe(III)-SPP at 303K	4.0	0.95	This work
SPP at 298K	4.0	0.12	This work
CuO- impregnated biochar	4.0	0.17	[61]
Magnetic orange peel biomass	6.0	1.08	[60]
Fe-impregnated *Citrus limetta* fruit waste	3.0	0.026	[59]
Fe(III) treated *Staphylococcus xylosus*	3.0	0.82	[58]
Ferric oxide modified Sugarcane bagasse	4.0	0.29	[57]
Fe(III) treated sawdust of spruce	6.0	0.13	[56]
Amorphous ZrO_2 nanoparticles	7.0	0.43	[55]
Aegle marmelous based magnetic biosorbent	3.0	0.93	[53]
Fe_2O_3 modified jute fiber	3.0	0.64	[54]
Zr(IV)-based magnetic sorbent	2.6–3.3	0.60	[52]
Zr(IV) modified biochar	6.0	0.83	[51]
Fe–Zr binary oxide	7.0	0.61	[50]
Zr(IV) loaded orange waste	3.0	1.17	[37]

arsenic-polluted water.

3.3.4. Biosorption thermodynamics of As(V) ion

To determine the nature of biosorption and the spontaneousness of the reaction, thermodynamic variables such as Gibb's free energy change, entropy change, and enthalpy change must be determined. Thermodynamic variables governing As(V) biosorption onto Fe(III)-SPP are determined from the temperature dependent isotherm studies. The value of equilibrium constants at different temperatures is determined by using a series of biosorption tests at varying concentrations of As(V) and Langmuir isotherm modeling. Since the unit of equilibrium constant used for thermodynamic calculation should be dimensionless, however, the Langmuir equilibrium constant (b) in the present biosorption system has the unit of L/mmoL which can be converted into the dimensionless equilibrium constant (K_{equ}) by the equation (equation (23)) described elsewhere as [62,63].

$$K_{equ} = b * 55.5 * 1000 \tag{23}$$

Where b (L/mmol) is the experimental equilibrium constant derived from the Langmuir isotherm model and 55.5 is the moles of water. The dimentionless equilibrium constant (K_{equ}) is related to ΔG° of the particular reaction by the relation as [31].

$$\Delta G^{\circ} = -RT\ln\left(K_{equ}\right) \tag{24}$$

Similarly, the ΔG°, ΔH°, and ΔS° are related to eachother from the following equation as [31,64].

$$\Delta G^{\circ} = \Delta H^{\circ} - T\Delta S^{\circ} \tag{25}$$

Now equating equations (24) and (25) we have

$$\ln\left(K_{equ}\right) = -\Delta H^{\circ} / RT + \Delta S^{\circ} / R \tag{26}$$

where, ΔG°, ΔH°, and ΔS° are respectively the standard free energy, enthalpy, and entropy change, respectively. The value of ΔG° at different temperatures was determined directly using equation (25)whereas the value of ΔH° and ΔS° are determined from the plot of $\ln(K_{equ})$ *versus* 1/T (Fig. 4(f)) and the evaluated values are listed in Table 4. As can be seen, the negative values of ΔG° rise with rising temperature (-18.40 ± 1.89, -19.98 ± 1.38, and -21.01 ± 1.52 kJ/mol at temperatures 298, 303, and 308K, respectively) indicating that the biosorption process is spontaneous and feasible [31,36,65]. As(V) biosorption onto Fe(III)-SPP has been analyzed to have a positive ΔH° value (58.24 kJ/mol), which clearly implies that biosorption is endothermic. Estimated value of positive ΔS° (0.26 kJ/mol K) indicates the increase of disorderness in the solid-solution interface, which might be due to the fact that the biosorption reaction of As(V) occurred with the release of some ions or molecules (in this case hydroxyl/or water ligand) that help to increase the randomness in the interfacial region. Similar types of thermodynamic behaviors were also observed from previous studies for the biosorption of As(V) onto La(III) loaded watermelon rind [31].

3.3.5. Effect of interfering ions

The naturally contaminated water with arsenic not only includes arsenic anions as a hazardous pollutant but also has other coexisting ions such as calcium (Ca^{2+}), sodium (Na^{+}), chloride (Cl^{-}), nitrate/nitrite (NO_2^-/NO_3^-), bicarbonate (HCO_3^-), phosphate (PO_4^{3-}), and sulphate (SO_4^{2-}) which may potentially suppress the biosorption performance of arsenic anion. The batch biosorption studies were carried out using Fe(III)-SPP to study the interfering effect of these anions for As(V) biosorption with the outcomes shown in Fig. 5. From this result, the uptake capacity of As(V) is influenced in the presence of these co-existing ions in the following order: $PO_4^{3-} > SO_4^{2-} > CO_3^{2-} > NO_2^-/NO_3^- \approx Cl^- > Na^+ \approx Ca^{2+}$. The cationic species such as Ca(II) and Na(I) had no or negligible interference whereas anionic species reduced biosorption performance depending on the nature of anions. The mono-valent species like Cl^-, and NO_3^- has very little or insignificant interference with the uptake of As(V) ion. Bicarbonate (HCO_3^-) had a moderate effect, whereas high concentrations of co-existing SO_4^{2-} and PO_4^{3-} significantly reduced As(V) biosorption capability of investigated Fe(III)-SPP biosorbent. Such a drop of As(V) uptake in co-existing system of SO_4^{2-} and PO_4^{3-} might be due to their high charge and affinity with loaded Fe(III) exist in Fe(III)-SPP biosorbent, which further makes it more favorable for the enhancement of competing effect with As(V).

3.4. Desorption of As(V) and biosorbent regeneration for further usage

A desorption study is necessary for biosorbent recycling and As(V) ion recovery. Since the As(V) biosorption was effective in acidic pH whereas it was insignificant at basic conditions, indicating that the application of acidic solution for As(V) desorption may not be effective. Therefore, neutral (1 M NaCl) and basic (1 M NaOH) solutions are chosen for a preliminary experiment that desorbed 43%

Table 4
Thermodynamic parameters determined for the sorption of As(V) onto Fe(III)-SPP

Adsorbent	T (1/K)	b × 10^4 (L/mmol)	K_C	ΔG°(kJ/mol)	ΔH°(kJ/mol)	ΔS°(kJ/mol K)
SPP	298 ± 1	356.68	1979.61	−18.8 ± 2.16	58.24 ± 2.31	0.26 ± 0.04
Fe(III)-SPP	293 ± 1	344.12	1909.92	−18.4 ± 1.89		
Fe(III)-SPP	298 ± 1	574.71	3189.65	−19.98 ± 1.38		
Fe(III)-SPP	303 ± 1	756.57	4199.01	−21.01 ± 1.52		

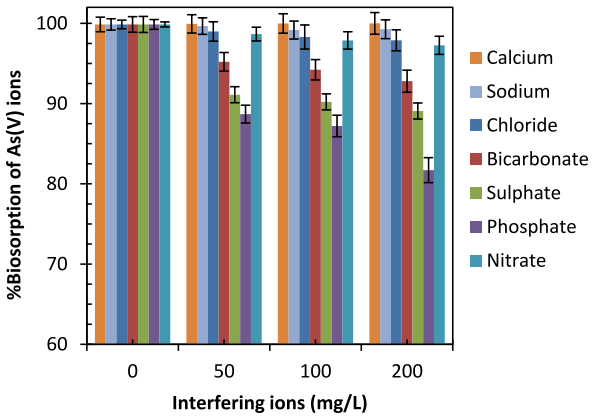

Fig. 5. Influence of interfering ions for the biosorption of As(V) onto Fe(III)-SPP.
(Conditions: arsenic concentration = 0.065 mmol/L, volume of solution = 25 mL, weight of biosorbent = 40 mg, pH = 4, shaking time = 24 h, shaking speed = 200 rpm and temperature = 298K).

and 98% of As(V), respectively. As a result, various concentrations of NaOH are utilized for further optimization, as illustrated in Fig. 6. It is apparent that, the percentage desorption increase as NaOH concentration rose and eventually reached 97% at 0.1 M NaOH. The % desorption is not more than 98.7% even using 1.5 M NaOH. Thus, the desorption of As(V) anions using 0.1 M NaOH solution is optimum for effective desorption of arsenic ion. It is inferred that the adsorbed As(V) anion is desorbed by the ligand substitution mechanism between As(V) anion from As(V)–Fe(III)-SPP and hydroxyl ion (OH^-) from NaOH solution as shown in Scheme 1 (step 4). After desorption, the spent biosorbent is regenerated after water washing and drying. It can be expected to be used instead of fresh Fe (III)-SPP for As(V) biosorption as shown in Scheme 1 (step 5), which will be tested in near future. The results show that the As(V) biosorbed by Fe(III)-SPP can be desorbed easily by dilute alkali (NaOH) solution and the biosorbent may be regenerated for further usage. A similar observation was observed for the desorption of fluoride from F–Zr(IV)-SOJR using lime water and KOH [66].

3.5. *Application of Fe(III)-SPP for the removal of arsenic from contaminated groundwater samples*

Nearly one-half of the Nepalese population in the Terai region is dependent on groundwater. Eight districts among 20 in the Terai region have groundwater containing high level of arsenic than the WHO recommended level (10 μg/L) for drinking water. There is no option for the people of these areas except this arsenic-polluted groundwater for drinking especially in the lower belt of Nawalparasi, Rupandehi, Parsa, Bara, and Banke districts. We have collected the groundwater samples of 3 different tubewells from the Nawalparasi district and their major chemical constituents and physico-chemical parameters are determined as shown in Table 5. The physico-chemical parameters such as pH, total hardness, nitrate (NO_3^-), total suspended solid (TSS), chloride (Cl^-), fluoride (F^-), sulphate

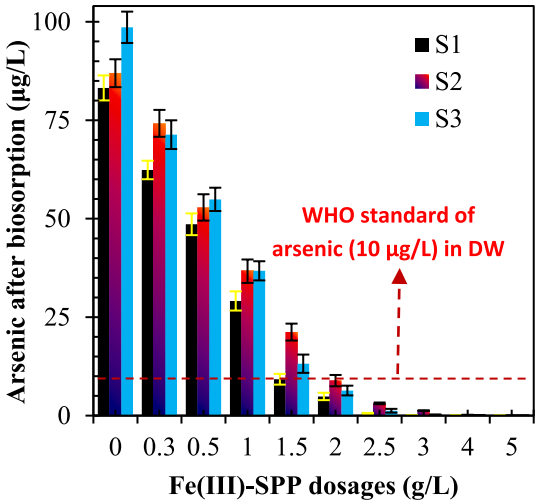

Fig. 6. Application of investigated Fe(III)-SPP for the treatment of arsenic from contaminated water.
(Conditions: arsenic concentration = (sample 1: S1 = 83.21 μg/L, sample 2: S2 = 86.94 μg/L, sample 3: S3 = 98.6 μg/L), volume of water = 10 mL, native pH of arsenic polluted water = (S1 = 7.12, S2 = 7.17, S3 = 6.93), shaking time = 24 h, shaking speed = 200 rpm and temperature = 298K).

(SO_4^{2-}), iron (Fe), calcium (Ca^{2+}), and sodium (Na^+) are found to be in the tolerance level but the concentration of arsenic are 8.6, 8.3, and 9.8 times higher for sample S1, S2, and S3, respectively. The remaining arsenic concentration in the examined samples of arsenic-polluted water is depicted in Fig. 7 as a function of Fe(III)-SPP dosage. It demonstrates that utilizing 1 g/L of biosorbent for each of the three analyzed water samples resulted in residual arsenic levels that were less than the Nepalese drinking water standard (50 μg/L) and its level is further decreasing with increasing Fe(III)-SPP amounts. More interestingly, the examined Fe(III)-SPP successfully reduced the arsenic concentration below the WHO recommended threshold limit by using 2 g/L, and complete removal of arsenic from polluted water was accomplished by usingFe(III)-SPP dosage higher than 4 g/L. In light of this, the study established the argument that the Fe (III)-SPP examined in this work might be a material that could be used to cure an aqueous solution that had been contaminated with trace levels of arsenic ions.

3.6. Dynamic biosorption of As(V) in a fixed bed column of Fe(III)-SPP

Fig. 8 shows the breakthrough profile of As(V) biosorption in a packed column of Fe(III)-SPP in continuous mode at three different bed heights. The results demonstrated that the breakthrough time is directly proportional to bed heights. The different parameters obtained from dynamic experiment are listed in Table 6 together with experimental conditions. Effluent volume (Eff_{volume}), the mass of As(V) uptake (q_{total}), and mass transfer zone (Δt) were found to increase with increasing bed height which is because As(V) has more biosorption sites available at higher doses of Fe(III)-SPP, which requires larger times for breakthrough. The determination of breakthrough behavior in a packed column is necessary for the proper design of a fixed bed biosorption column. The column capacity of the Fe(III)-SPP bed decreased with increasing height of the biosorbent bed which may be due to the short contact and possibility of channeling between the As(V) ion and active sites. The low biosorption capacity of Fe(III)-SPP for As(V) in fixed bed system compared to batch mode is due to the insufficient contact time for bisorption process. A similar nature of fluoride biosorption was also observed by Paudyal et al. in packed column of Zr(IV)-DOJR [67].

3.7. Modeling of data obtained from dynamic sorption in fixed bed column

The best-fitted dynamic model and feasible column parameters are usually investigated for the effective design of the biosorption column in a fixed bed system. The data obtained from fixed bed biosorption columns are often described by using Bohart-Adams, Thomas, and Yoon-Nelson models and in most circumstances, they can accurately represent breakthrough curves and design parameters for the fixed bed column system.

3.7.1. Thomas model

The Thomas model is one of the most extensively used models to describe the dynamic biosorption process in a fixed bed system. During the biosorption process, mass transfer at the contact is assumed to regulate the majority of the biosorption. The following equation serves as a representation of the Thomas model's linear expression [68]:

$$\ln\left(\frac{C_i}{C_t}-1\right)=k_{Th}\frac{q_0 M}{F}-k_{Th}C_i\times t \tag{27}$$

where M is the mass of Fe(III)-SPP packed in the column (g), F is the flow rate of As(V) solution through the column (mL/min), and qo is the maximum biosorption capacity of As(V) in packed column system (mmol/g). The values of k_{Th} and q_0 are determined using the slope and intercept of the straight line determined from the plot of ln ((C_i/C_t) - 1) *vs* t (Fig. 9(a)). Table 7 lists the Thomas parameters that have been tested for the biosorption of As(V) onto the Fe(III)-SPP bed. The high value of coefficient of determination ($R^2 > 0.97$) obtained for all three-bed depth shows that the Thomas model and experimental results are well-matched. The maximum column capacity obtained from the Thomas model (q_0, mmol/g) and rate constant (k_{Th}) were found to be higher at lower bed height. This can

Table 5
Evaluated physiochemical parameters of the arsenic polluted ground water collected from different parts of Nawalparasi district, Lumbini Province, Nepal.

Physiochemical parameters	Samples			WHO limit
	S1	S2	S3	
pH	7.12	7.17	6.93	6.5–8.5
Total hardness (mg/L)	397	383	314.54	300
Total dissolved solid (TDS, mg/L)	612.82	594.98	608.67	<300
Total suspended solids (TSS, mg/L)	51.9	39.4	54.36	100
Chloride (mg/L)	207	187	186.68	250
Fluoride (mg/L)	0.53	0.68	0.72	1.5
Sulphate (mg/L)	48.35	40.13	46.87	250
Nitrite/Nitrate (mg/L)	9.22	6.15	3.26	50
Phosphate (mg/L)	2.27	1.29	4.28	–
Iron (mg/L)	0.97	0.74	0.81	0.3
Calcium (mg/L)	23.97	11.38	31.59	100
Total arsenic (μg/L)	86.94	83.21	98.64	10

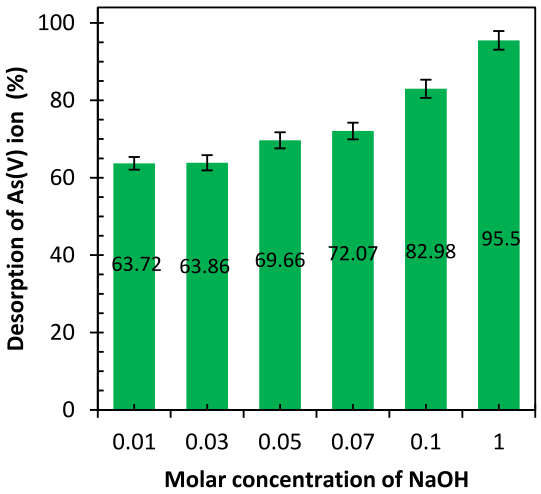

Fig. 7. Desorption of As(V) from As(V)-loaded Fr(III)-SPP using NaOH solution.
(**Conditions:** amount of As(V) sorbed onto Fe(III)-SPP = 0.005 mmol/g, weight of As(V) loaded Fe(III)-SPP = 50 mg, volume of NaOH = 10 mL, shaking time = 24 h, shaking speed = 200 rpm and temperature = 298K).

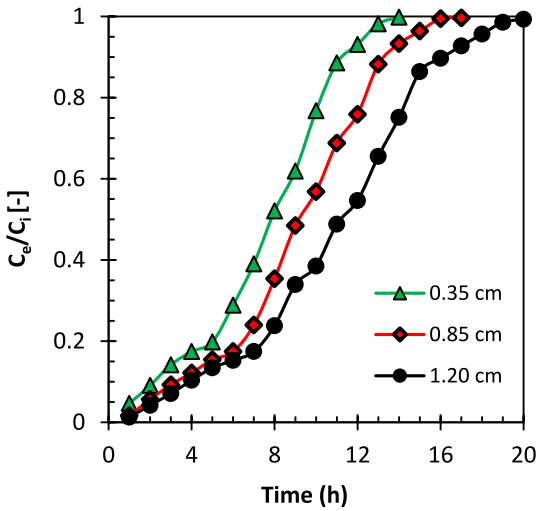

Fig. 8. Biosorption of As(V) onto fixed bed column of Fe(III)-SPP in continuous mode at different bed depth (**Conditions:** As(V) solution = 0.061 mmol/L, pH = 4, flow rate = 150 mL/h, particle size = <150 μm, and temperature = rt (291±2K)).

Table 6
Column parametrs evaluated for the biosorption of As(V) onto fixed bed column packed with Fe(III)-SPP

Experimental conditions					Evaluated dynamic arameters in fixed bed column			
C_i (mmol/L)	pH	M (mg)	F (mL/h)	Z (cm)	Eff_{Volume} (mL)	Δt (h)	q_{total} (mmol)	q_{colum} (mmol/g)
0.061	4 ± 0.2	75	150 ± 5	1.20	3000 ± 121	12	0.98 ± 0.002	0.17 ± 0.003
0.061	4 ± 0.2	50	150 ± 5	0.85	2550 ± 128	13	0.84 ± 0.001	0.22 ± 0.004
0.061	4 ± 0.2	25	150 ± 5	0.35	2100 ± 125	15	0.72 ± 0.003	0.38 ± 0.003

be reasonably described due to the lack of channeling and exposure of most of the active sites in Fe(III)-SPP with As(V) ion, whereas % of active sites exposed to As(V) are low in higher bed height due to the channeling effect.

3.7.2. Bohart-Adams model

In cases where the effluent concentration is lower, this model is more effective. The biosorption rate is proportional to the solids' residual capacity and the concentration of the biosorbent according to Bohart–Adam's model. It can be expressed in the linear form as

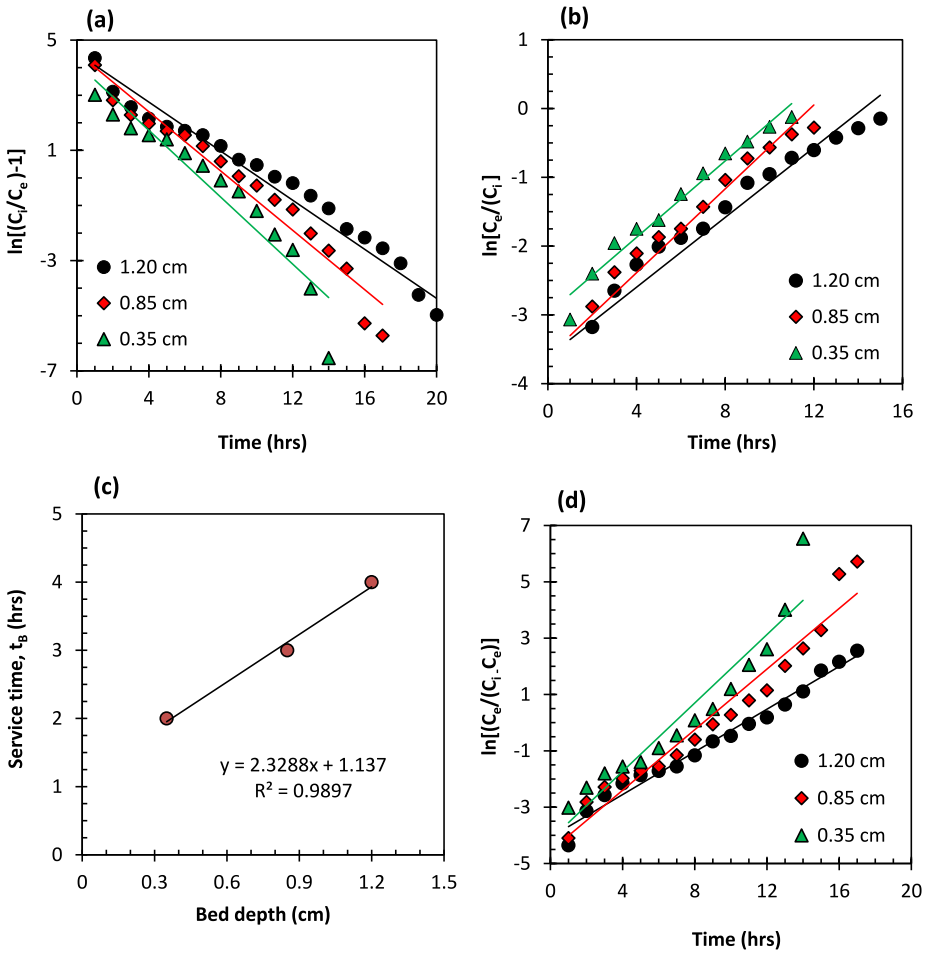

Fig. 9. Modeling of data obtained from the biosorption of As(V) onto fixed bed column of Fe(III)-SPP (a) Thomas model, (b) Adams-Bohrt's model, (c) BDST model and (d) Yoon Nelson model.

Table 7
Column parameters evaluated for the sorption of As(V) ion (0.061 mmol/L, at pH 4) onto the bed of Fe(III)-SPP using Thomas, Yoon-Nnelson and Adam-Bohart modeling.

Z (cm)	Thomas parameters		Yoon Nelson parameters				Adam-Bohart parameters		
	q_0 (mmol/g)	k_{Th} (L/mmol h)	R^2	τ (h)	K_{YN} (1/h)	R^2	N_0 (g/L)	K_{AB} (L/mmol h)	R^2
1.20	0.19 ± 0.03	725 ± 5.97	0.96	0.14	0.37 ± 0.08	0.95	5.53 ± 0.25	298 ± 2.18	0.86
0.85	0.22 ± 0.05	877 ± 4.21	0.95	0.11	0.53 ± 0.06	0.94	6.31 ± 0.37	364 ± 3.86	0.88
0.35	0.38 ± 0.02	990 ± 7.44	0.90	0.09	0.60 ± 0.05	0.90	10.40 ± 0.21	371 ± 3.61	0.93

[69]:

$$ln\left(\frac{C_t}{C_i}\right) = k_{AB}C_i \times t_b - \frac{N_0}{U_0}k_{AB}Z \tag{28}$$

where C_i is the initial concentration (mmol/L) of As(V); C_t is the concentration (mmol/L) of As(V) at time t; k_{AB} is the Bohart–Adams model rate constant (L/h); N_0 is the column saturation concentration (mmol/L); Z is the height of the bed (cm) in a column. From the slope and intercept of ln(C_e/C_i)-1) *versus* t (Fig. 9(b)), the values of the Bohart-Adams parameters k_{AB} and N_0 were calculated which are listed in Table 7. The Bohart-Adams rate constant was found to decrease with increasing bed depth. When the bed height increased, the saturation concentration (N_0) of the column increased which is reasonably attributed to the increase of active biosorption sites at higher mass of biosorbent. The validity of the Bohart-Adams model for the biosorption of As(V) onto the fixed-bed column of Fe(III)-SPP is confirmed from the value of coefficient of determination (R^2) which is greater than 0.86 for all bed heights studied. To show the relationship between the effective service time or time required for breakthrough and bed depth, equation (28) is rearranged in a

simple mathematical form which can describe the initial portion of the breakthrough curves as [70].

$$t_b = \frac{N_0 Z}{C_i U_0} - \frac{1}{k_{AB} C_i} ln\left(\frac{C_i}{C_b} - 1\right) \quad (29)$$

where C_b is breakthrough concentration (mmol/L) of As(V) ion. The plot of breakthrough time (t_b) versus bed depth (Z) gives the straight line plot (Fig. 9(c)) so that it is also called the bed depth service time (BDST) model. The linear relationship between the breakthrough time and bed depth with $R^2 > 0.98$ ensured the validity of the BDST model and explains the high efficiency of the Fe(III)-SPP bed for the examined As(V) biosorption.

3.7.3. Yoon-Nelson model

According to the Yoon-Nelson model, the rate of biosorption for each adsorbate molecule is proportional to the probability of biosorbate breakthrough onto the biosorbent bed. The following linear equation can be used to represent this model [71].

$$ln\left(\frac{C_t}{C_i} - 1\right) = k_{YN} t - \tau k_{YN} \quad (30)$$

where k_{YN}, and $\boldsymbol{\tau}$ (tau) are Yoon-Nelson rate constant (min^{-1}), and time needed for 50% biosorbate breakthrough (h), respectively. The values of Yoon-Nelson model parameters like k_{YN} and, $\boldsymbol{\tau}$ are also shown in Table 7, which are determined by plotting ln ((C_t/C_i)-1) with t (Fig. 9(d)) and obtaining from the slope and intercept of this linear plot. The Yoon-Nelson rate constant (k_{YN}) decreases with decreasing bed height. Because there are fewer active sites available for As(V) biosorption as bed height (mass of biosorbent) decreases thus there are less number of interactions between As(V) anion and active sites, which lowers the Yoon-Nelson rate constant. Moreover, the increase of $\boldsymbol{\tau}$ value (time required for 50% breakthrough) observed at higher bed height is also due to the increase of active biosorption sites at higher mass. The value of the coefficient of determination (R^2) obtained in this case is higher than 0.90 for all the bed heights. So that this model can well describe the experimental data of As(V) biosorption in a packed column of Fe(III)-SPP.

The design parameter of the fixed bed system are necessary for the application of investigated biosorption system in actual practice. Therefore, utilizing the well-known Bohart-Adams, Thomas, BDST, and Yoon-Nelson models, the design parameters for the biosorption reactor and biosorption capabilities of the examined system are assessed.

The Bohart-Adams model is only relevant at the beginning of the breakthrough curve, whereas the Thomas, BDST, and Yoon Nelson models are found to be useful for better explanation of column data for the explored biosorption system.

4. Conclusion

In the present work, saponification followed by Fe(III) loading was used for the creation of anion exchange sites in Pomelo peel biomass for effective biosorption of As(V) from water. Biosorbent characterizations were done using SEM, EDX, XRD, and FTIR together with mass titration for pH_{PZC} determination to obtain information on active site creation and As(V) biosorption. As(V) biosorption by Fe(III)-SPP significantly depends on solutions' pH, agitation time, amount of As(V) ion, and Fe(III)-SPP dosage. Langmuir isotherm and PSO kinetics models both provided good fits to the experimental data. Highest As(V) uptake capacity of Fe(III)-SPP was determined to be 0.72, 0.86, and 0.95 mmol/g at temperatures 293, 298, and 303K, respectively using Langmuir isotherm modeling. The coordinated water and hydroxyl ligands that existed on the coordination sphere of iron in Fe(III)-SPP are considered to be substituted by As(V) ions during the biosorption process. The existence of co-existing Na^+ and Ca^{2+} have no interference, Cl^- and NO_3^- have negligible interferences, whereas SO_4^{2-} and PO_4^{3-} caused the suppression of As(V) uptake capacity of Fe(III)-SPP. The trace amount of arsenic that existed in polluted groundwater could be successfully reduced to the WHO-set threshold limit (10 μg/L) using a small amount of investigated Fe(III)-SPP. The spontaneous and endothermic nature of As(V) biosorption could be concluded from the evaluated values of negative ΔG^0 and positive ΔH^0, respectively. Higher than 95% desorption of As(V) from As(V) loaded Fe(III)-SPP could be achieved by using 0.1 M NaOH. As(V) biosorption using a fixed bed column shows that Fe(III)-SPP could be effective also in the continuous mode. Thus, it is anticipated that this research would open up new avenues for the production of affordable Fe(III)-SPP biosorbent for arsenic that might be a promising substitute for the treatment of aqueous solution contaminated with arsenic from water/wastewate.

Declarations

Author contribution statement

Deepak Gyawali, Sangita Rijal: Performed the experiments; Wrote the paper.

Prabin Basnet, Megh Raj Pokhrel: Analyzed and interpreted the data.

Kedar Nath Ghimire: Conceived and designed the experiments; Analyzed and interpreted the data.

Hari Paudyal: Conceived and designed the experiments; Analyzed and interpreted the data; Contributed reagents, materials, analysis tools or data; Wrote the paper.

Funding statement

Mrs. Sangita Rijal, one of the authors of this paper, would like to thank UGC, Nepal for granting a student grant (MRS-75/76-S&T-29) and conducted the preliminary experiment for this research work.

Data availability statement

Data will be made available on request.

Declaration of interest's statement

The authors declare no conflict of interest.

Acknowledgments

Dr. Khag Raj Sharma and Dr. Sabita Shrestha of the Central Department of Chemistry at Tribhuvan University in Kirtipur, Kathmandu, Nepal, are gratefully acknowledged by all the authors of this study for FTIR measurements. Authors would like to heartly thanks to Dr. Bhanu Bhaktta Neupane and Dr. Bipeen Dahal, Central Department of Chemistry for the help of similarity checking using Turnitin software and SEM images, respectively.

Appendix A. Supplementary data

Supplementary data to this article can be found online at https://doi.org/10.1016/j.heliyon.2023.e13465.

References

[1] K. Jomova, Z. Jenisova, M. Feszterova, S. Baros, J. Liska, D. Hudecova, J. Rhodes, M. Valko, Arsenic: toxicity, oxidative stress and human disease, J. Appl. Toxicol. 31 (2) (2011) 95–107, https://doi.org/10.1002/jat.1649.
[2] M.J. Uddin, Y.K. Jeong, Review: efficiently performing periodic elements with modern adsorption technologies for arsenic removal, Environ. Sci. Pollut. Res. 27 (32) (2020) 39888–39912, https://doi.org/10.1007/s11356-020-10323-z.
[3] D.N. Nhiem, D.H. Duc, D.T. Lim, N.Q. Bac, P.N. Chuc, D.T. Dung, N.T.H. Chi, N.N. Pham, N.V.N. Mai, T.X. Mau, D.Q. Khieu, Strong adsorption of arsenite and phosphate from aqueous solution using La_2O_3–CeO_2 composite, J. Polym. Environ. 29 (2021) 1310–1323, https://doi.org/10.1007/s10924-020-01967-6.
[4] D. Mohan, C.U. Pittman, Arsenic removal from water/wastewater using adsorbents-A critical review, J. Hazard Mater. 142 (1–2) (2007) 1–53, https://doi.org/10.1016/j.jhazmat.2007.01.006.
[5] M.S. Karmacharya, V.K. Gupta, I. Tyagi, S. Agarwal, V.K. Jha, Removal of as (III) and as (V) using rubber tirederived activated carbon modified with alumina composite, J. Mol. Liq. 216 (2016) 836–844, https://doi.org/10.1016/j.molliq.2016.02.025.
[6] W. Wong, H.Y. Wong, A.B.M. Badruzzaman, H.H. Goh, M. Zaman, Recent advances in the exploitation of nanomaterial for arsenic removal from water: a review, Nanotechnol. (4) (2017), 042001, https://doi.org/10.1088/1361-6528/28/4/042001.
[7] H. Tajernia, T. Ebadi, B. Nasernejad, M. Ghafori, Arsenic removal from water by sugarcane bagasse: an application of response surface methodology (RSM), Water, Air, Soil Pollut. 225 (7) (2014), https://doi.org/10.1007/s11270-014-2028-4.
[8] M. Rajendran, D. Thangavelu, Removal of as (V) from water using galvanically coupled sacrificial metals, J. Hazard Mater. 409 (2021), 124564, https://doi.org/10.1016/j.jhazmat.2020.124564.
[9] S. Karki, R.L. Aryal, S. Bhattarai, S.K. Gautam, B.R. Poudel, Adsorptive Removal of Arsenic (III) from aqueous solution using chemically-modified sweet lime (*Citrus limetta*) peels, J. Nepal Chem. Soc. 37 (2017) 11–19, https://doi.org/10.3126/jncs.v37i0.32044.
[10] S. Wang, B. Gao, A.R. Zimmerman, Y. Li, L. Ma, W.G. Harris, K.W. Migliaccio, Removal of arsenic by magnetic biochar prepared frompinewood and natural hematite, Bioresour. Technol. 175 (2015) 391–395, https://doi.org/10.1016/j.biortech.2014.10.104.
[11] M.F. Naujokas, B. Anderson, H. Ahsan, H.V. Aposhian, J.H. Graziano, C. Thompson, W.A. Suk, The broad scope of health effects from chronic arsenic exposure: update on a worldwide public health problem, Environ. Health Perspect. 121 (3) (2013) 295–302, https://doi.org/10.1289/ehp.1205875.
[12] J. Podgorski, M. Berg, Global threat of arsenicin groundwater, Science 368 (2020) 845–850, https://doi.org/10.1126/science.aba1510.
[13] Z. Yan, Global solutions to a silent poison, Science 368 (2020) 818–819, https://doi.org/10.1126/science.abb9746.
[14] T. Davydiuk, X. Chen, L. Huang, Q. Shuai, X.C. Le, Removal of inorganic arsenic from water using metal organic frameworks, J. Environ. Sci. 97 (2020) 162–168, https://doi.org/10.1016/j.jes.2020.08.012.
[15] Q.L. Zhang, Y.C. Lin, X. Chen, N.Y. Gao, A method for preparing ferric activated carbon composite adsorbents to remove arsenic from drinking water, J. Hazard Mater. 148 (2007) 671–678, https://doi.org/10.1016/j.jhazmat.2007.03.026.
[16] J.S. Uppal, Q. Zheng, X.C. Le, Arsenic in drinking water-recent examples and updates from Southeast Asia, Curr. Opin. Environ. Sci. Health 7 (2019) 126–135, https://doi.org/10.1016/j.coesh.2019.01.004.
[17] Y. Yu, L. Yu, K.Y. Koh, C. Wang, J.P. Chen, Rare-earth metal based adsorbents for effective removal of arsenic from water: a critical review, Crit. Rev. Environ. Sci. Technol. 48 (22–24) (2019) 1127–1164, https://doi.org/10.1080/10643389.2018.1514930.
[18] K. Taleb, J. Markovski, Z. Velickovic, J. Rusmirovic, M. Rancic, V. Pavlovic, A. Marinkovic, Arsenic removal by magnetite-loaded amino modified nano/microcellulose adsorbents: effect of functionalization and media size, Arab. J. Chem. 12 (8) (2019) 675–4693, https://doi.org/10.1016/j.arabjc.2016.08.006.
[19] F. Hesami, B. Bina, A. Ebrahimi, M.M. Amin, Arsenic removal by coagulation using ferric chloride and chitosan from water, Int. J. Environ. Health Eng. 2 (2013) 17. https://www.ijehe.org/text.asp?2013/2/1/17/110170.
[20] A. Ortega, I. Oliva, K.E. Contreras, I. González, M.R. Cruz-Díaz, E.P. Rivero, Arsenic removal from water by hybrid electro-regenerated anion exchange resin/electrodialysis process, Separ. Purif. Technol. 184 (2017) 319–326, https://doi.org/10.1016/j.seppur.2017.04.050.
[21] A. Abejon, A. Garea, A. Irabien, Arsenic removal from drinking water by reverse osmosis: minimization of costs and energy consumption, Separ. Purif. Technol. 144 (2015) 46–53, https://doi.org/10.1016/j.seppur.2015.02.017.
[22] R.Y. Ning, Arsenic removal by reverse osmosis, Desalination 143 (2002) 237–241, https://doi.org/10.1016/S0011-9164(02)00262-X.

[23] L. Hao, M. Liu, N. Wang, G. Li, A critical review on arsenic removal from water using iron-based adsorbents, RSC Adv. 8 (2018) 39545–39560, https://doi.org/10.1039/C8RA08512A.

[24] D.E. Giles, M. Mohapatra, T.B. Issa, S. Anand, P. Singh, Iron and aluminum based adsorption strategies for removing arsenic from water, J. Environ. Manag. 92 (12) (2011) 3011–3022, https://doi.org/10.1016/j.jenvman.2011.07.018.

[25] H. He, F. Deng, T. Shen, L. Yang, D. Chen, J. Luo, X. Luo, X. Min, F. Wang, Exceptional adsorption of arsenic by zirconium metal-organic frameworks: engineering exploration and mechanism insight, J. Colloid Interface Sci. 539 (2019) 223–234, https://doi.org/10.1016/j.jcis.2018.12.065.

[26] K.N. Ghimire, K. Inoue, H. Yamaguchi, K. Makino, T. Miyajima, Adsorptive separation of arsenate and arsenite anions from aqueous medium by using orange waste, Water Res. 37 (20) (2003) 4945–4953, https://doi.org/10.1016/j.watres.2003.08.029.

[27] K.R. Raj, A. Kardam, S. Srivastava, Development of polyethyleneimine modified Zea mays as a high capacity biosorbent for the removal of as (III) and as (V) from aqueous system, Int. J. Miner. Process. 122 (2013) 66–70, https://doi.org/10.1016/j.minpro.2013.02.010.

[28] N.K. Niazi, E.D. Burton, Arsenic sorption to nanoparticulate mackinawite (FeS): an examination of phosphate competition, Environ. Pollut. 218 (2016) 111–117, https://doi.org/10.1016/j.envpol.2016.08.031.

[29] V.M. Boddu, K. Abburi, J.L. Talbott, E.D. Smith, R. Haasch, Removal of arsenic (III) and arsenic (V) from aqueous medium using chitosan-coated biosorbent, Water Res. 42 (3) (2008) 633–642, https://doi.org/10.1016/j.watres.2007.08.014.

[30] H. Paudyal, B. Pangeni, K. Inoue, H. Kawakita, K. Ohto, K.N. Ghimire, H. Harada, S. Alam, Adsorptive removal of trace concentration of fluoride ion from water by using dried orange juice residue, Chem. Eng. J. 223 (2013) 844–853, https://doi.org/10.1016/j.cej.2013.03.055.

[31] R.L. Aryal, A. Thapa, B.R. Poudel, B. Dahal, H. Paudyal, K.N. Ghimire, Effective biosorption of arsenic from water using La(III) loaded carboxyl functionalized watermelon rind, Arab. J. Chem. 15 (1) (2021), 103674, https://doi.org/10.1016/j.arabjc.2021.103674.

[32] N. Ayawei, A. Newton Ebelegi, D. Wankasi, Modeling and interpretation of adsorption isotherms, J. Chem. (2017), 3039817, https://doi.org/10.1155/2017/3039817, 2017.

[33] P.Z. Aksu, S.S. Cagatay, F. Gonen, Continuous fixed bed biosorption of reactive dyes by dried Rhizopus arrhizus: determination of column capacity, J. Hazard Mater. 143 (2007) 362–371, https://doi.org/10.1016/j.jhazmat.2006.09.039.

[34] K.N. Ghimire, K. Inoue, K. Makino, T. Miyajima, Adsorptive removal of arsenic using orange juice residue, Separ. Sci. Technol. 37 (2002) 2785–2799, https://doi.org/10.1081/SS–120005466.

[35] H. Paudyal, B. Pangeni, K.N. Ghimire, K. Inoue, H. Kawakita, K. Ohto, S. Alam, Adsorption behavior of orange waste gel for some rare earth ions and its application to the removal of fluoride from water, Chem. Eng. J. 195–196 (2012) 289–296, https://doi.org/10.1016/j.cej.2012.04.061.

[36] B.R. Poudel, R.L. Aryal, S. Bhattarai, A.R. Koirala, S.K. Gautam, K.N. Ghimire, B. Pant, M. Park, H. Paudyal, M.R. Pokhrel, Agro-waste derived biomass impregnated with TiO_2 as a potential adsorbent for removal of as (III) from water, Catalysts 10 (2020) 1125, https://doi.org/10.3390/catal10101125.

[37] B.K. Biswas, J.I. Inoue, K. Inoue, K.N. Ghimire, H. Harada, K. Ohto, H. Kawakita, Adsorptive removal of as (V) and as (III) from water by a Zr (IV)-loaded orange waste gel, J. Hazard Mater. 154 (2008) 1066–1074, https://doi.org/10.1016/j.jhazmat.2007.11.030.

[38] M. Chiban, G. Carja, G. Lehutu, F. Sinan, Equilibrium and thermodynamic studies for the removal of as (V) ions from aqueous solution using dried plants as adsorbents, Arab. J. Chem. 9 (2016) S988–S999, https://doi.org/10.1016/j.arabjc.2011.10.002.

[39] S. Lagergren, Zur theorie der sogenannten adsorption geloester stoffe Veternskapsakad, J. Hand Surg. Br. Vol. 24 (4) (1898) 1.

[40] J.P. Simonin, On the comparison of pseudo-first order and pseudo-second order rate laws in the modeling of adsorption kinetics, Chem. Eng. J. 300 (2016) 254–263, https://doi.org/10.1016/j.cej.2016.04.079.

[41] G. Blanchanchard, M. Maunaye, G. Marti, Removal of heavy metal from water by means of natural zeolites, Water Res. 18 (2) (1984) 1501–1507.

[42] Y.S. Ho, Review of second-order models for adsorption systems, J. Hazard Mater. 136 (3) (2006) 681–689, https://doi.org/10.1016/j.jhazmat.2005.12.043.

[43] W.J. Weber Jr., J.C. Morris, Kinetics of adsorption on carbon from solution, J.Sanit Eng. ASCE 89 (1963) 31–59.

[44] I. Langmuir, The constitution and fundamental properties of solids and liquids, J. Am. Chem. Soc. 38 (1916) 2221–2295, https://doi.org/10.1021/ja02268a002.

[45] D. Mondal, G.J.F. Cruz, J. Rimaycuna, K. Soukup, M.M. Gómez, J.L. Solis, J. Lang, Agro waste derived biochars impregnated with ZnO for removal of arsenic and lead in water, J. Environ. Chem. Eng. 8 (3) (2020), 103800, https://doi.org/10.1016/j.jece.2020.103800.

[46] H. Freundlich, Uber die adsorption in losungen, J. Phys. Chem. 57 (1906) 385–470.

[47] J. Wang, X. Guo, Adsorption isotherm models: classification, physical meaning, application and solving method, Chemosphere 258 (2020), 127279, https://doi.org/10.1016/j.chemosphere.2020.127279.

[48] M.A. Al-Ghouti, D.A. Daana, Guidelines for the use and interpretation of adsorption isotherm models: a review, J. Hazard Mater. 393 (2020), 122383, https://doi.org/10.1016/j.jhazmat.2020.122383.

[49] S.J. Peighambardoust, R. Foroutan, S.H. Peighambardoust, H. Khatooni, B. Ramavandi, Decoration of *Citrus limon*wood carbon with Fe_3O_4 to enhanced Cd^{2+} removal: a reclaimable and magnetic nanocomposite, Chemosphere 282 (2021), 131088.

[50] Z. Ren, G. Zhang, J.P. Chen, Adsorptive removal of arsenic from water by an iron–zirconium binary oxide adsorbent, J. Colloid Interface Sci. 358 (2011) 230–237, https://doi.org/10.1016/j.jcis.2011.01.013.

[51] M.A. Rahman, D. Lamb, M.M. Rahman, M.M. Bahar, P. Sanderson, S. Abbasi, A.F. Bari, R. Naidu, Removal of arsenate from contaminated waters by novel zirconium and zirconium-iron modified biochar, J. Hazard Mater. 409 (2021), 124488, https://doi.org/10.1016/j.jhazmat.2020.124488.

[52] Y.M. Zheng, S.F. Lim, J.P. Chen, Preparation and characterization of zirconium-based magnetic sorbent for arsenate removal, J. Colloid Interface Sci. 338 (2009) 22–29, https://doi.org/10.1016/j.jcis.2009.06.021.

[53] U.K. Sahu, S. Sahu, S.S. Mahapatra, R.K. Patel, Synthesis and characterization of magnetic bio-adsorbent developed from Aegle marmelos leave for removal of as (V) from aqueous solutions, Environ. Sci. Pollut. Res. 26 (2019) 946–958, https://doi.org/10.1007/s11356-018-3643-1.

[54] U.K. Sahu, S. Sahu, S.S. Mahapatra, R.K. Patel, Synthesis and characterization of an eco-friendly composite of jute fiber and Fe_2O_3 nanoparticles and its application as an adsorbent for removal of as (V) from water, J. Mol. Liq. 237 (2017) 313–321, https://doi.org/10.1016/j.molliq.2017.04.092.

[55] H. Cui, Q. Li, S. Gao, J.K. Shang, Strong adsorption of arsenic species by amorphous zirconium oxide nanoparticles, J. Ind. Eng. Chem. 18 (2012) 1418–1427, https://doi.org/10.1016/j.jiec.2012.01.045.

[56] M. Urik, P. Littera, M. Kolen, Removal of arsenic (V) from aqueous solutions using chemically modified sawdust of spruce (Picea abies): kinetics and isotherm studies, Int. J. Environ. Sci. Technol. 6 (2009) 451–456, https://doi.org/10.1007/BF03326084.

[57] E. Pehlivan, H.T. Tran, W.K.I. Ouédraogo, C. Schmidt, D. Zachmann, M. Bahadir, Sugarcane bagasse treated with hydrous ferric oxide as a potential adsorbent for the removal of as (V) from aqueous solutions, Food Chem. 138 (2013) 133–138, https://doi.org/10.1016/j.foodchem.2012.09.110.

[58] M. Aryal, M. Ziagova, M. Liakopoulou-Kyriakides, Study on arsenic biosorption using Fe (III)-treated biomass of Staphylococcus xylosus, Chem. Eng. J. 162 (2010) 178–185, https://doi.org/10.1016/j.cej.2010.05.026.

[59] L. Verma, M.A. Siddique, J. Singh, R.N. Bharagava, As(III) and As(V) removal by using iron impregnated biosorbents derived from waste biomass of Citrus limmeta (peel and pulp) from the aqueous solution and groundwater, J. Environ. Manag. 250 (2019), 109452, https://doi.org/10.1016/j.scitotenv.2018.06.170.

[60] F. Meng, B. Yang, B. Wang, S. Duan, Z. Chen, W. Ma, Novel dendrimer-like magnetic biosorbent based on modified orange peel waste: adsorption-reduction behavior of arsenic, ACS Sustain. Chem. Eng. 5 (2017) 9692–9700, https://doi.org/10.1021/acssuschemeng.7b01273.

[61] M. Imran, M.M. Iqbal, J. Iqbal, N.S. Shah, Z.U.H. Khan, B. Murtaza, M. Amjad, S. Ali, M. Rizwan, Synthesis, characterization, and application of novel MnO and CuO impregnated biochar composites to sequester arsenic (As) from water: modeling, thermodynamics, and reusability, J. Hazard Mater. 401 (2021), 123338, https://doi.org/10.1016/j.jhazmat.2020.123338.

[62] X. Zhou, X. Zhou, The unit problem in the thermodynamic calculation of adsorption using Langmuir equation, Chem. Eng. Commun. 201 (2014) 1459–1467, https://doi.org/10.1080/00986445.2013.818541.

[63] L. Xu, Y. Liu, J. Wang, Y. Tang, Z. Zhang, Selective adsorption of Pb^{2+} and Cu^{2+} on amino-modified attapulgite: kinetic, thermal dynamic and DFT studies, J. Hazard Mater. 404 (2021), 124140, https://doi.org/10.1016/j.jhazmat.2020.124140.

[64] R.A. Reza, M. Ahmaruzzaman, Comparative study of waste derived adsorbents for sequestering methylene blue from aquatic environment, J. Environ. Chem. Eng. 3 (2014) 395–404. https://doi:10.1016/j.jece.2014.06.006.
[65] H.N. Tran, S.J. You, A. Hosseini-Bandegharaei, H.P. Chao, Mistakes and inconsistencies regarding adsorption of contaminants from aqueous solutions: a critical review, Water Res. 120 (2017) 88–116, https://doi.org/10.1016/j.watres.2017.04.014.
[66] H. Paudyal, K. Ohto, H. Kawakita, K. Inoue, Recovery of fluoride from water through adsorption using orange–waste gel, followed by desorption using saturated lime water, J. Mater. Cycles Waste Manag. 22 (2020) 1484–1491, https://doi.org/10.1007/s10163-020-01042-1.
[67] H. Paudyal, B. Pangeni, K. Inoue, H. Kawakita, K. Ohto, S. Alam, Adsorptive removal of fluoride from aqueous medium using a fixed bed column packed with Zr (IV) loaded dried orange juice residue, Bioresour. Technol. 146 (2013) 713–720, https://doi.org/10.1016/j.biortech.2013.07.014.
[68] H.C. Thomas, Heterogeneous ion exchange in a flowing system, J. Am. Chem. Soc. 66 (1944) 1664–1666.
[69] G. Bohart, E.N. Admas, Some aspects of the behavior of charcoal with respect to chlorine, J. Am. Chem. Soc. 42 (1920) 523–544.
[70] S. Sadaf, H.N. Bhatti, Evaluation of peanut husk as a novel, low cost biosorbent for the removal of indosol orange RSN dye from aqueous solutions: batch and fixed bed studies, Clean Technol. Environ. Policy 16 (2014) 527–544, https://doi.org/10.1007/s10098-013-0653-z.
[71] Y.H. Yoon, J.H. Nelson, Application of gas adsorption kinetics: a theoretical model for respirator cartridge service life, Am. Ind. Hyg. Assoc. J. 45 (1984) 509–516.